CHAPTER
3

Remote-Sensing Antennas

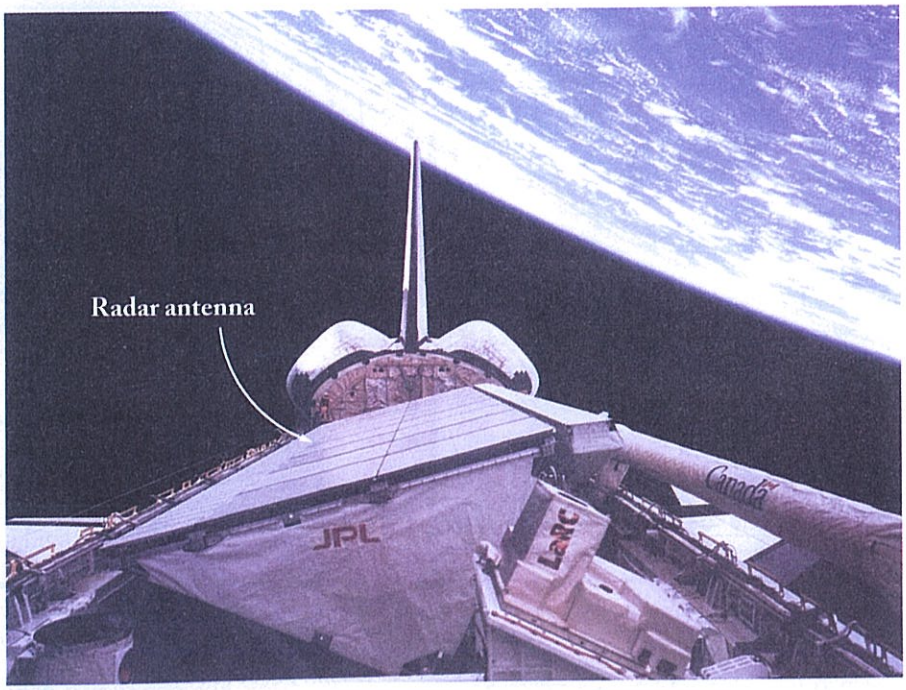

12 m long SIR-C radar antenna carried by the Space Shuttle

CONTENTS

Overview

The ***antenna*** of a microwave remote-sensing system is one of the most important elements of the overall system. It defines the ground area illuminated by its beam, and through its properties—radiation pattern, gain, radiation efficiency, polarization purity, etc.—it influences the quality of the data measured by the sensor. This book assumes that the reader has general familiarity with how antennas transmit and receive EM waves. Accordingly, the first part of this chapter provides a general review of antennas, and the latter part focuses on the type of antennas commonly used by microwave sensing systems, both active and passive.

▶ An antenna is a transducer that converts a guided wave propagating on a transmission line into an electromagnetic wave propagating in an unbounded medium (usually free space), or vice versa. ◀

Figure 3-1 shows how a wave is launched by a hornlike antenna, with the horn acting as the transition segment between the waveguide and free space. Antennas are made in various shapes and sizes (Fig. 3-2). The radiation and impedance properties of an antenna are governed by its shape, size, and material properties, and its dimensions are usually measured in units of λ of the wave it is launching or receiving; a 1 m long dipole antenna operating at a wavelength $\lambda = 2$ m exhibits the same properties as a 1 cm long dipole operating at $\lambda = 2$ cm. Hence, in most of our discussions in this chapter, we refer to antenna dimensions in wavelength units.

Reciprocity

The directional function characterizing the *relative* distribution of power radiated by an antenna is known as the ***antenna radiation pattern***, or simply the ***antenna pattern***. An ***isotropic*** antenna is a hypothetical antenna that radiates equally in all directions, and it is often used as a reference radiator when describing the radiation properties of real antennas.

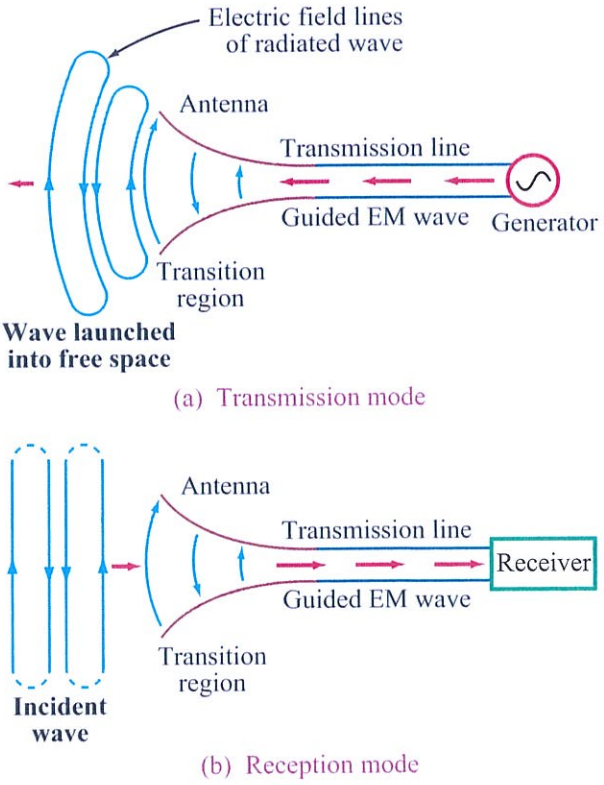

Figure 3-1: Antenna as a transducer between a guided electromagnetic wave and a free-space wave, for both transmission and reception.

▶ Most antennas are ***reciprocal*** devices, exhibiting the same radiation pattern for transmission as for reception. ◀

Reciprocity means that if in the transmission mode a given antenna transmits in direction A 100 times the power it transmits in direction B, then when used in the reception mode it is 100 times more sensitive to electromagnetic radiation incident from direction A than from B. All the antennas shown in Fig. 3-2 obey the reciprocity law, but not all antennas are reciprocal devices. Reciprocity may not hold for some solid-state antennas composed of nonlinear semiconductors or ferrite materials, as discussed in Section 3-12. The

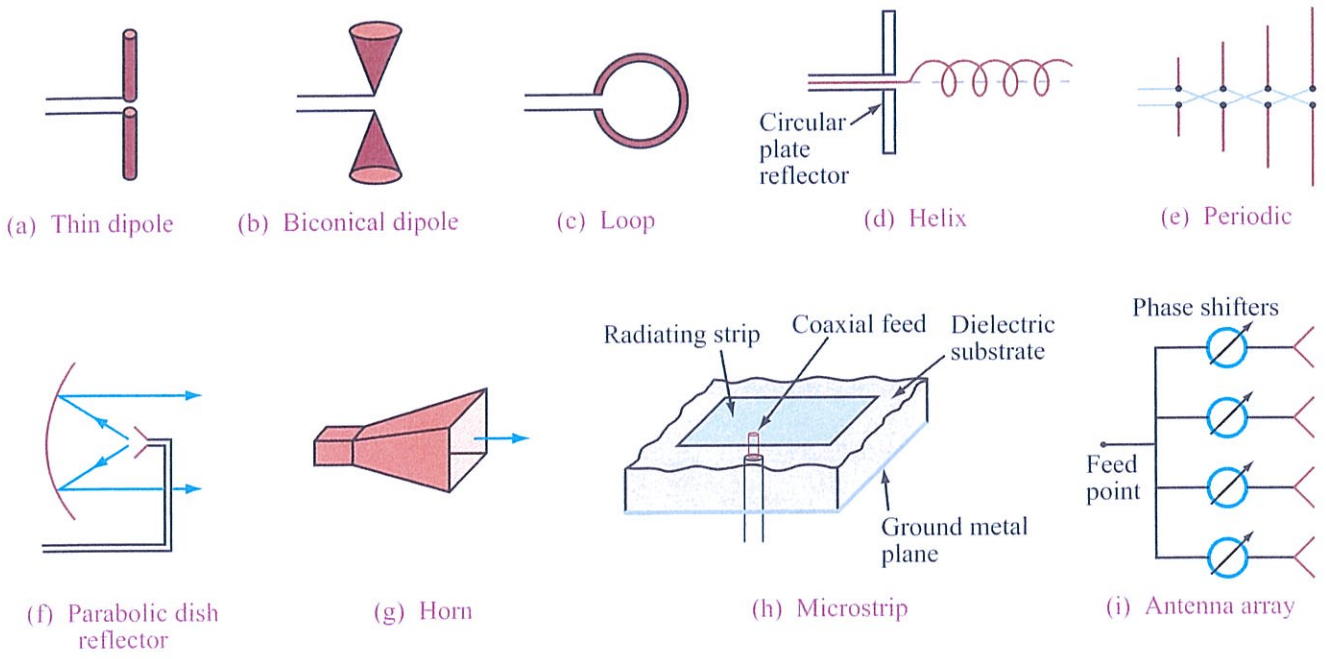

Figure 3-2: Various types of antennas.

reciprocity property is very convenient because it allows us to compute the radiation pattern of an antenna in the transmission mode, even when the antenna is intended to operate as a receiver. Reciprocity is assumed throughout Sections 3-1 to 3-11.

> ► As a reciprocal device, an antenna operating in the receiving mode extracts from an incident wave only that component of the wave whose electric field matches the antenna polarization state. ◄

Another important reciprocity property is ***antenna impedance***, which pertains to the transfer of power from a generator to the antenna when the antenna is used as a transmitter and, conversely, the transfer of power from the antenna to a load when the antenna is used as a receiver. Throughout this chapter, it is assumed that the antenna is properly matched to the transmission line connected to its terminals, thereby avoiding reflections and their associated problems.

Radiation sources

Radiation sources fall into two categories: conduction currents and aperture fields. The dipole and loop antennas [Fig. 3-2(a) and (c)] are examples of current sources; the time-varying currents flowing in the conducting wires give rise to the radiated electromagnetic fields. A horn antenna [Fig. 3-2(g)] is an example of the second group because the electric and magnetic fields across the horn's aperture serve as the sources of the radiated fields. The aperture fields are themselves induced by time-varying currents on the surfaces of the horn's walls, and therefore ultimately all radiation is due to time-varying currents. The choice of currents or apertures as the sources is merely a computational convenience arising from the structure of the antenna. We briefly examine the radiation processes associated with both types of sources.

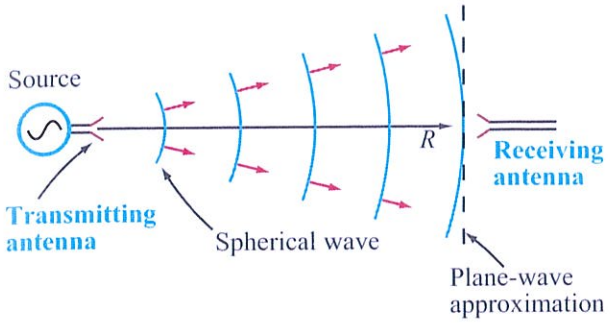

Figure 3-3: Far-field plane-wave approximation.

Far-field region

The wave radiated by a point source is spherical in nature, with the wavefront expanding outward at a rate equal to the phase velocity u_p (or the velocity of light c if the medium is free space). If R, the distance between the transmitting antenna and the receiving antenna, is sufficiently large such that the wavefront across the receiving aperture may be considered planar (Fig. 3-3), then the receiving aperture is said to be in the ***far-field*** (or ***far-zone***) region of the transmitting point source. This region is of particular significance because for most applications, the location of the observation point is indeed in the far-field region of the antenna. The far-field plane-wave approximation allows the use of certain mathematical approximations that simplify the computation of the radiated field and, conversely, provide convenient techniques for synthesizing the appropriate antenna structure that gives rise to the desired far-field antenna pattern.

By convention, the ***far-field distance*** is defined as the distance R from the antenna at which the maximum error between the phase of the spherical wave radiated by the antenna and the phase of its plane-wave approximation is $\pi/8$. For an antenna whose longest linear dimension is d, the far-field distance is

$$R \geq 2d^2/\lambda \qquad \textbf{(far-field distance)}, \tag{3.1}$$

where λ is the wavelength of the wave radiated by the antenna.

Antenna arrays

When multiple antennas operate together, the combination is called an ***antenna array*** [Fig. 3-2(i)], and the array as a whole behaves as if it were a single antenna. By controlling the magnitude and phase of the signal feeding each antenna, it is possible to *shape the radiation pattern* of the array and to *electronically steer the direction of the beam.* These topics are treated in Sections 3-8 to 3-10.

3-1 The Hertzian Dipole

By regarding a linear antenna as consisting of a large number of infinitesimally short conducting elements, each of which is so short that current may be considered uniform over its length, the field of the entire antenna may be obtained by integrating the fields from all these differential antennas, with the proper magnitudes and phases taken into account. A short linear antenna of length $l \ll \lambda$ is known as a ***Hertzian dipole***.

The wire oriented along the z direction in Fig. 3-4 carries a sinusoidally varying current given by

$$i(t) = I_0 \cos \omega t = \Re\mathfrak{e}[I_0 e^{j\omega t}] \qquad \text{(A)}, \tag{3.2}$$

where I_0 is the current amplitude and ω is the angular frequency. From Eq. (3.2), the phasor current $I = I_0$. Even though the current has to go to zero at the two ends of the dipole, we treat it as constant across its entire length.

To characterize the directional character of the radiated power at a fixed distance R from the antenna, antenna pattern plots usually are presented in a spherical coordinate system (Fig. 3-5). Its variables, R, θ, and ϕ, are called the ***range***, ***zenith angle***, and ***azimuth angle***, respectively. In the far-field region, the expressions for the electric and magnetic fields of the wave radiated by the Hertzian dipole in a medium with wavenumber k are given by

$$\mathbf{E} = \hat{\boldsymbol{\theta}} \frac{jI_0 lk\eta_0}{4\pi} \left(\frac{e^{-jkR}}{R}\right) \sin\theta \quad \text{(V/m)}, \tag{3.3}$$

$$\mathbf{H} = \hat{\boldsymbol{\phi}} \frac{E_\theta}{\eta_0} \qquad \text{(A/m)}. \tag{3.4}$$

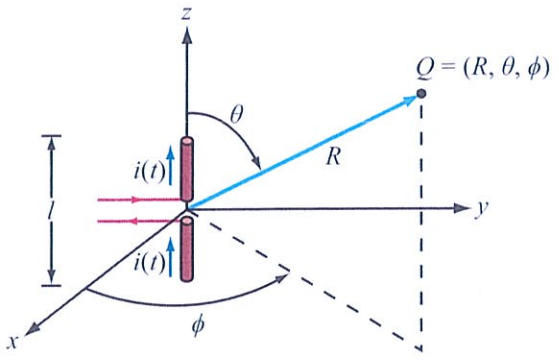

Figure 3-4: Short dipole placed at the origin of a spherical coordinate system.

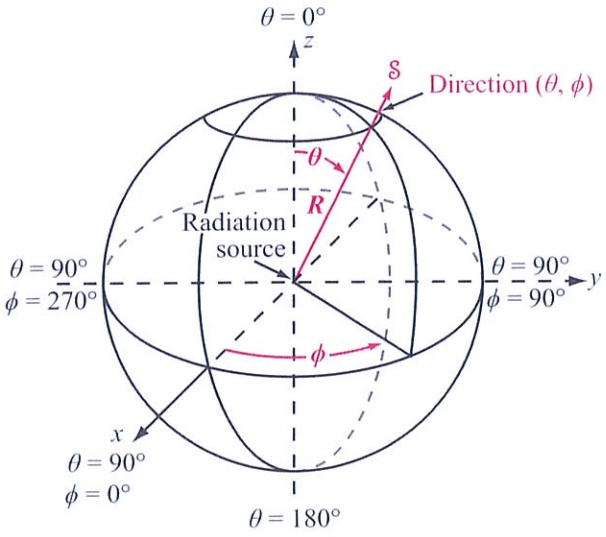

Figure 3-5: Spherical coordinate system.

At the observation point Q (Fig. 3-4), the wave is similar to a uniform plane wave with its electric and magnetic fields in phase, related by the intrinsic impedance of the medium η_0, and their directions orthogonal to each other and to the direction of propagation $\hat{\mathbf{R}}$. Both fields are proportional to $\sin\theta$ and independent of ϕ (which is expected from symmetry considerations).

Given $\mathbf{E}$ and $\mathbf{H}$, the ***time-averaged power density*** of the radiated wave is obtained by applying Eq. (2.71); that is,

$$\mathcal{S} = \tfrac{1}{2}\mathfrak{Re}(\mathbf{E} \times H^*) \qquad (\text{W/m}^2). \tag{3.5}$$

For the short dipole, use of Eqs. (3.3) and (3.4) yields

$$\mathcal{S} = \hat{\mathbf{R}}\,\mathcal{S}(R, \theta), \tag{3.6}$$

with

$$\begin{aligned} \mathcal{S}(R, \theta) &= \left(\frac{\eta_0 k^2 I_0^2 l^2}{32\pi^2 R^2}\right) \sin^2\theta \\ &= \mathcal{S}_0 \sin^2\theta \qquad (\text{W/m}^2). \end{aligned} \tag{3.7}$$

The directional pattern of an antenna is described by its ***normalized radiation intensity*** $F(\theta, \phi)$, defined as the ratio of the power density $\mathcal{S}(R, \theta, \phi)$ at a specified range R to $\mathcal{S}_{\max}$, the maximum value of $\mathcal{S}(R, \theta, \phi)$ at the same range,

$$F(\theta, \phi) = \frac{\mathcal{S}(R, \theta, \phi)}{\mathcal{S}_{\max}} \qquad \textbf{(dimensionless)}. \tag{3.8}$$

For the Hertzian dipole, the $\sin^2\theta$ dependence in Eq. (3.7) indicates that the radiation is maximum in the broadside direction ($\theta = \pi/2$), corresponding to the azimuth plane, and is given by

$$\begin{aligned} \mathcal{S}_{\max} = \mathcal{S}_0 &= \frac{\eta_0 k^2 I_0^2 l^2}{32\pi^2 R^2} \\ &= \frac{15\pi I_0^2}{R^2}\left(\frac{l}{\lambda}\right)^2 \qquad (\text{W/m}^2), \end{aligned} \tag{3.9}$$

where use was made of the relations $k = 2\pi/\lambda$ and $\eta_0 \approx 120\pi$. We observe that $\mathcal{S}_{\max}$ is directly proportional to I_0^2 and l^2 (with l measured in wavelengths), and that it decreases with distance as $1/R^2$.

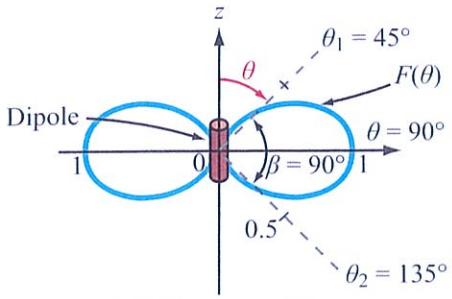

(a) Elevation pattern

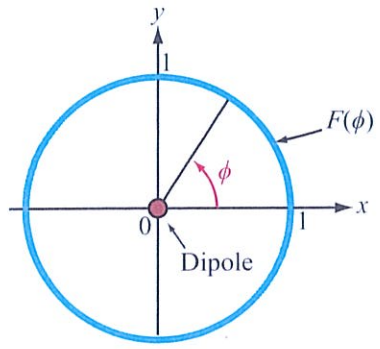

(b) Azimuth pattern

Figure 3-6: Radiation patterns of a short dipole.

From the definition of the normalized radiation intensity given by Eq. (3.8), it follows that

$$F(\theta, \phi) = F(\theta) = \sin^2 \theta. \qquad (3.10)$$

Plots of $F(\theta)$ are shown in Fig. 3-6 in both the elevation plane (the θ plane) and the azimuth plane (ϕ plane).

▶ No energy is radiated by the short dipole along the direction of the dipole axis and maximum radiation ($F = 1$) occurs in the ***broadside direction*** ($\theta = 90°$). Since $F(\theta)$ is independent of ϕ, the pattern is doughnut-shaped in θ–ϕ space. ◀

3-2 Antenna Radiation Characteristics

▶ An ***antenna pattern*** describes the far-field directional properties of an antenna when measured at a fixed distance from the antenna. By virtue of reciprocity, a receiving antenna has the same directional antenna pattern as the pattern that it exhibits when operated in the transmission mode. ◀

In general, the antenna pattern is a three-dimensional plot that displays the strength of the radiated field or power density as a function of direction, with direction being specified by the zenith angle θ and the azimuth angle ϕ.

Consider a transmitting antenna placed at the origin of the observation sphere shown in Fig. 3-7. The differential power radiated by the antenna through an elemental area dA is

$$dP_{\text{rad}} = \mathcal{S} \cdot d\mathbf{A} = \mathcal{S} \cdot \hat{\mathbf{R}}\, dA = \mathcal{S}\, dA \qquad \text{(W)}, \qquad (3.11)$$

where $\mathcal{S}$ is the radial component of the time-average power density $\mathcal{S}$. In the far-field region of any antenna, $\mathcal{S}$ is always in the radial direction. In a spherical

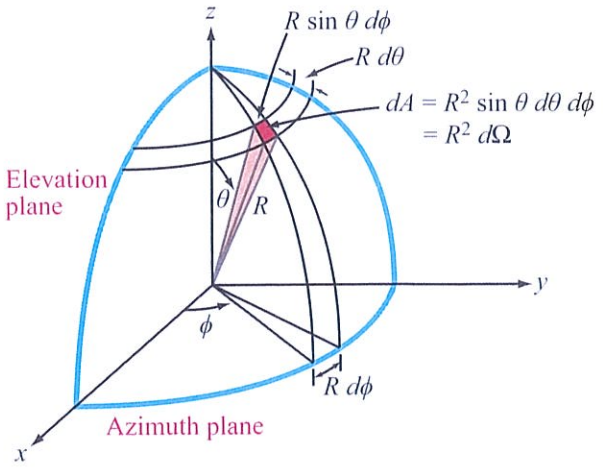

Figure 3-7: Definition of solid angle $d\Omega = \sin\theta\, d\theta\, d\phi$.

coordinate system,

$$dA = R^2 \sin\theta \, d\theta \, d\phi, \tag{3.12}$$

and the ***solid angle*** $d\Omega$ associated with dA, defined as the subtended area divided by R^2, is given by

$$d\Omega = \frac{dA}{R^2} = \sin\theta \, d\theta \, d\phi \qquad \text{(sr)}. \tag{3.13}$$

Note that whereas a planar angle is measured in radians and the angular measure of a complete circle is 2π (rad), a solid angle is measured in ***steradians*** (sr), and the angular measure for a spherical surface is $\Omega = (4\pi R^2)/R^2 = 4\pi$ (sr). The solid angle of a hemisphere is 2π (sr).

Using the relation $dA = R^2 \, d\Omega$, dP_{rad} can be rewritten as

$$dP_{\text{rad}} = R^2 \mathcal{S}(R,\theta,\phi) \, d\Omega. \tag{3.14}$$

The total power radiated by an antenna through a spherical surface at a fixed distance R is obtained by integrating Eq. (3.14) over that surface:

$$\begin{aligned} P_{\text{rad}} &= R^2 \int_{\phi=0}^{2\pi} \int_{\theta=0}^{\pi} \mathcal{S}(R,\theta,\phi) \sin\theta \, d\theta \, d\phi \\ &= R^2 \mathcal{S}_{\max} \int_{\phi=0}^{2\pi} \int_{\theta=0}^{\pi} F(\theta,\phi) \sin\theta \, d\theta \, d\phi \\ &= R^2 \mathcal{S}_{\max} \iint_{4\pi} F(\theta,\phi) \, d\Omega \qquad \text{(W)}, \end{aligned} \tag{3.15}$$

where $F(\theta,\phi)$ is the normalized radiation intensity defined by Eq. (3.8). The 4π symbol under the integral sign is used as an abbreviation for the indicated limits on θ and ϕ. Formally, P_{rad} is called the ***total radiated power***.

3-2.1 Antenna Pattern

Each specific combination of the zenith angle θ and the azimuth angle ϕ denotes a specific direction in the spherical coordinate system of Fig. 3-7.

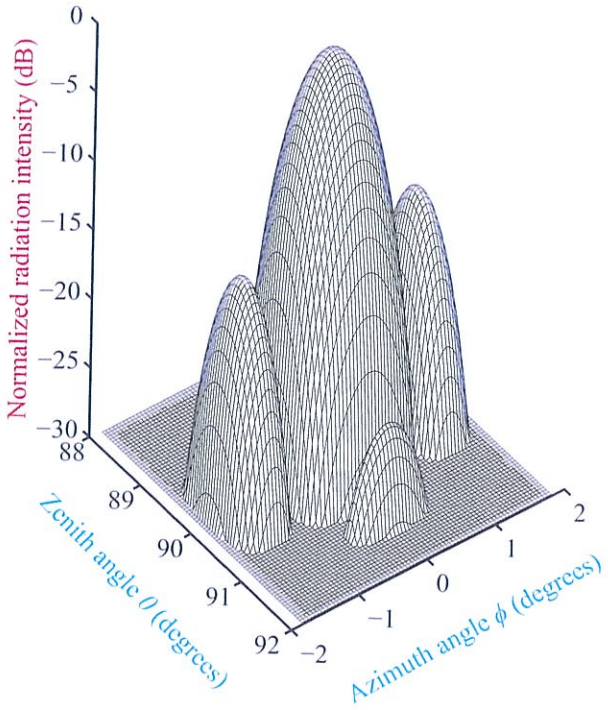

Figure 3-8: Three-dimensional pattern of a narrow-beam antenna.

▶ The normalized radiation intensity $F(\theta,\phi)$ characterizes the directional pattern of the energy radiated by the antenna. ◀

A plot of $F(\theta,\phi)$ as a function of both θ and ϕ constitutes a three-dimensional pattern, an example of which is shown in Fig. 3-8.

Often, it is of interest to characterize the variation of $F(\theta,\phi)$ in the form of two-dimensional plots in specific planes in the spherical coordinate system. The two planes most commonly specified for this purpose are the elevation and azimuth planes. The ***elevation plane***, also called the θ plane, is a plane corresponding to a constant value of ϕ. For example, $\phi = 0$ defines the x–z plane and $\phi = 90°$ defines the y–z plane, both of which are elevation planes (Fig. 3-7). A plot of $F(\theta,\phi)$ versus θ in either of these planes constitutes a two-dimensional pattern in the elevation plane. This is not to imply,

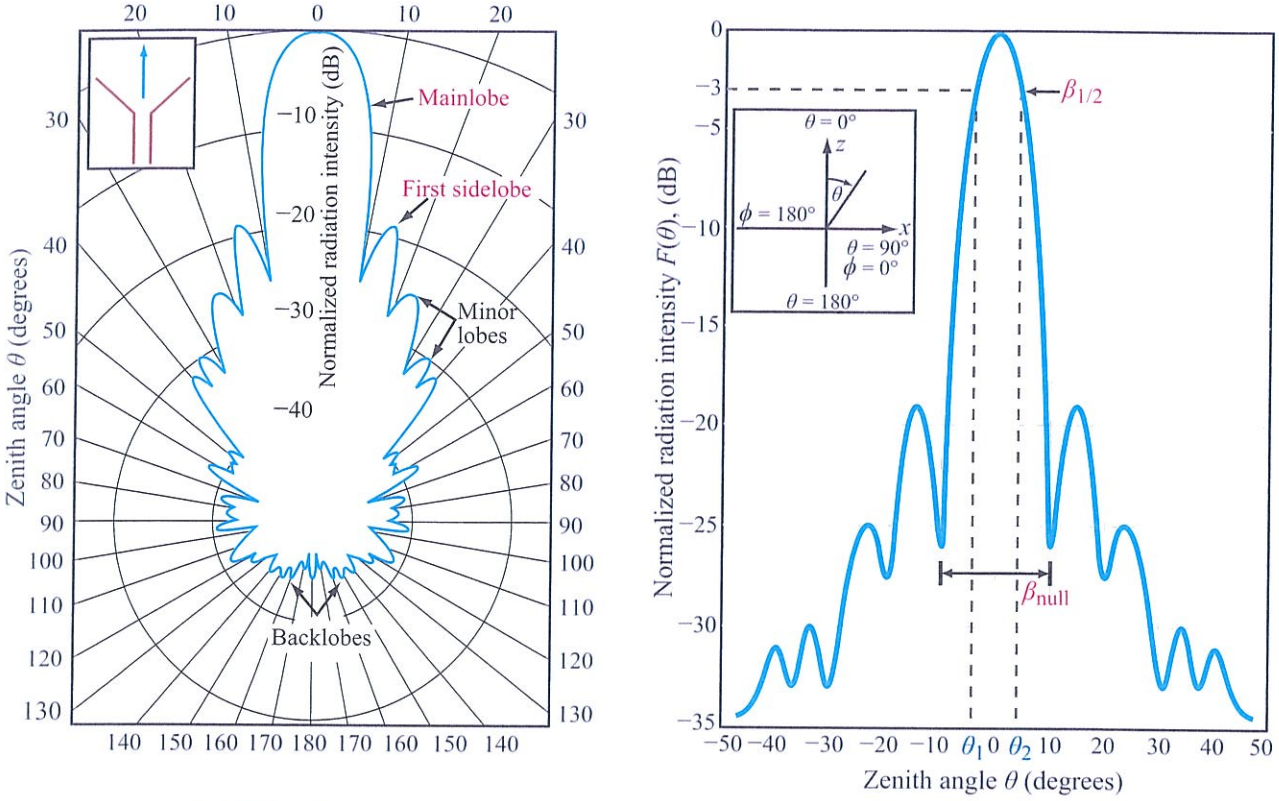

(a) Polar diagram (b) Rectangular plot

Figure 3-9: Representative plots of the normalized radiation pattern of a microwave antenna in (a) polar form and (b) rectangular form.

however, that the elevation-plane pattern is necessarily the same in all elevation planes.

The ***azimuth plane***, also called the ϕ plane, is specified by $\theta = 90°$ and corresponds to the x–y plane. The elevation and azimuth planes are often called the two ***principal planes*** of the spherical coordinate system.

Some antennas exhibit highly directive patterns with narrow beams, in which case it is often convenient to plot the antenna pattern on a decibel scale by expressing F in decibels:

$$F\ [\text{dB}] = 10 \log F.$$

As an example, the antenna pattern shown in Fig. 3-9(a) is plotted on a decibel scale in polar coordinates, with intensity as the radial variable. This format permits a convenient visual interpretation of the directional distribution of the ***radiation lobes***.

Another format commonly used for inspecting the pattern of a narrow-beam antenna is the rectangular display shown in Fig. 3-9(b), which permits the pattern to be easily expanded by changing the scale of the horizontal axis. These plots represent the variation in only one plane in the observation sphere, the $\phi = 0$ plane. Unless the pattern is symmetrical in ϕ, additional plots are required to define the overall variation of $F(\theta, \phi)$ with θ and ϕ.

Strictly speaking, the polar angle θ is always positive, being defined over the range from 0° (z direction) to 180° ($-z$ direction), and yet the θ axis in Fig. 3-9(b) is

shown to have both positive and negative values. This is not a contradiction, but rather a different form of plotting antenna patterns. The right-hand half of the plot represents the variation of F (dB) with θ as θ is increased in a clockwise direction in the x–z plane [see inset in Fig. 3-9(b)], corresponding to $\phi = 0$, whereas the left-hand half of the plot represents the variation of F (dB) with θ as θ is increased in a counterclockwise direction at $\phi = 180°$. Thus, a negative θ value simply denotes that the direction (θ, ϕ) is in the left-hand half of the x–z plane.

The pattern shown in Fig. 3-9(a) indicates that the antenna is fairly directive, since most of the energy is radiated through a narrow sector called the ***mainlobe***. In addition to the mainlobe, the pattern exhibits several ***sidelobes*** and ***backlobes*** as well. For most applications, these extra lobes are considered undesirable because they represent wasted energy for transmitting antennas and potential interference directions for receiving antennas.

3-2.2 Beam Dimensions

For an antenna with a single mainlobe, the ***pattern solid angle*** Ω_p describes the equivalent width of the mainlobe of the antenna pattern (Fig. 3-10). It is defined as the integral of the normalized radiation intensity $F(\theta, \phi)$ over a sphere:

$$\Omega_p = \iint_{4\pi} F(\theta, \phi)\, d\Omega \quad \text{(sr)}. \tag{3.16}$$

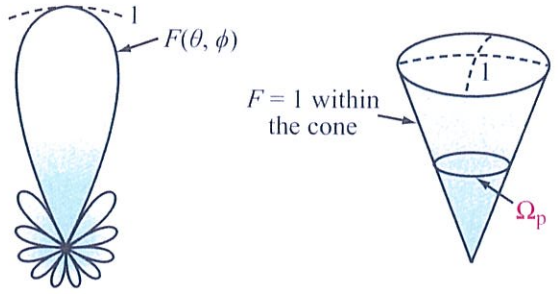

(a) Actual pattern (b) Equivalent solid angle

Figure 3-10: The pattern solid angle Ω_p defines an equivalent cone over which all the radiation of the actual antenna is concentrated with uniform intensity equal to the maximum of the actual pattern.

► For an isotropic antenna with $F(\theta, \phi) = 1$ in all directions, $\Omega_p = 4\pi$ (sr). ◄

The pattern solid angle characterizes the directional properties of the three-dimensional radiation pattern. To characterize the width of the mainlobe in a given plane, the term used is ***beamwidth***. The ***half-power beamwidth***, or simply the beamwidth β, is defined as the angular width of the mainlobe between the two angles at which the magnitude of $F(\theta, \phi)$ is equal to half of its peak value (or -3 dB on a decibel scale). For example, for the pattern displayed in Fig. 3-9(b), β is given by

$$\beta = \theta_2 - \theta_1, \tag{3.17}$$

where θ_1 and θ_2 are the ***half-power angles*** at which $F(\theta, 0) = 0.5$ (with θ_2 denoting the larger value and θ_1 denoting the smaller one, as shown in the figure). If the pattern is symmetrical and the peak value of $F(\theta, \phi)$ is at $\theta = 0$, then $\beta = 2\theta_2$. For the short-dipole pattern shown earlier in Fig. 3-6(a), $F(\theta)$ is maximum at $\theta = 90°$; θ_2 is at 135°, and θ_1 is at 45°. Hence, $\beta = 135° - 45° = 90°$. The beamwidth β is also known as the ***3 dB beamwidth***. In addition to the half-power beamwidth, other beam dimensions may be of interest for certain applications, such as the ***null beamwidth*** β_{null}, which is the angular width between the first nulls on the two sides of the peak [Fig. 3-9(b)].

3-2.3 Antenna Directivity

The ***peak directivity*** D of an antenna is defined as the ratio of its maximum normalized radiation intensity, F_{max} (which by definition is equal to 1), to the average

value of $F(\theta,\phi)$ over all directions (4π space):

$$D = \frac{F_{\max}}{F_{\text{av}}} = \frac{1}{\frac{1}{4\pi}\iint_{4\pi} F(\theta,\phi)\,d\Omega} = \frac{4\pi}{\Omega_{\text{p}}} \quad \textbf{(dimensionless)}. \tag{3.18}$$

Here Ω_{p} is the pattern solid angle defined by Eq. (3.16). Thus, the narrower Ω_{p} of an antenna pattern is, the greater is the directivity. For an isotropic antenna, $\Omega_{\text{p}} = 4\pi$; hence, its directivity $D_{\text{iso}} = 1$.

By using Eq. (3.15) in Eq. (3.18), D can be expressed as

$$D = \frac{4\pi R^2 \mathcal{S}_{\max}}{P_{\text{rad}}} = \frac{\mathcal{S}_{\max}}{\mathcal{S}_{\text{av}}}, \tag{3.19}$$

where $\mathcal{S}_{\text{av}} = P_{\text{rad}}/(4\pi R^2)$ is the average value of the radiated power density and is equal to the total power radiated by the antenna, P_{rad}, divided by the surface area of a sphere of radius R.

► Since $\mathcal{S}_{\text{av}} = \mathcal{S}_{\text{iso}}$, where $\mathcal{S}_{\text{iso}}$ is the power density radiated by an isotropic antenna, D represents the ratio of the maximum power density radiated by the antenna to the power density radiated by an isotropic antenna, both measured at the same range R and excited by the same amount of input power. ◄

Usually, D is expressed in decibels:* $D\,[\text{dB}] = 10\log D$.

For an antenna with a single mainlobe pointing in the z direction as shown in Fig. 3-11, Ω_{p} may be approximated as the product of the half-power beamwidths β_{xz} and β_{yz} (in radians):

$$\Omega_{\text{p}} \approx \beta_{xz}\beta_{yz}, \tag{3.20}$$

and therefore

$$D = \frac{4\pi}{\Omega_{\text{p}}} \approx \frac{4\pi}{\beta_{xz}\beta_{yz}}. \tag{3.21}$$

*A note of caution: Even though we often express certain dimensionless quantities in decibels, we should always convert their decibel values to natural values before using them in the relations given in this chapter.

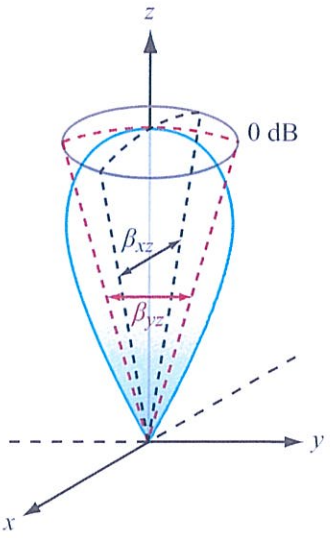

Figure 3-11: The solid angle of a unidirectional radiation pattern is approximately equal to the product of the half-power beamwidths in the two principal planes; that is, $\Omega_{\text{p}} \approx \beta_{xz}\beta_{yz}$.

Although approximate, this relation provides a useful method for estimating the antenna directivity from measurements of the beamwidths in the two orthogonal planes whose intersection is the axis of the mainlobe.

For a Hertzian dipole, application of Eq. (3.18) with $F(\theta) = \sin^2\theta$ [from Eq. (3.10)] gives

$$D = \frac{4\pi}{\displaystyle\iint_{4\pi} F(\theta,\phi)\sin\theta\,d\theta\,d\phi} = \frac{4\pi}{\displaystyle\int_{\phi=0}^{2\pi}\int_{\theta=0}^{\pi} \sin^3\theta\,d\theta\,d\phi} = \frac{4\pi}{8\pi/3} = 1.5$$

or, equivalently, 1.76 dB.

3-2.4 Antenna Gain

Of the total power P_{t} (transmitter power) supplied to the antenna, a part, P_{rad}, is radiated out into space, and the remainder, P_{loss}, is dissipated as heat in the antenna

structure. The ***radiation efficiency*** ξ is defined as the ratio of P_{rad} to P_t:

$$\xi = \frac{P_{rad}}{P_t} \qquad \textbf{(dimensionless)}. \tag{3.22}$$

The ***peak gain*** of an antenna is defined as

$$G = \frac{4\pi R^2 \mathcal{S}_{max}}{P_t}, \tag{3.23}$$

which is similar in form to the expression given by Eq. (3.19) for the directivity D except that it is referenced to the input power supplied to the antenna, P_t, rather than to the radiated power P_{rad}. In view of Eq. (3.22),

$$G = \xi D \qquad \textbf{(dimensionless)}. \tag{3.24}$$

► The gain accounts for ohmic losses in the antenna material, whereas the directivity does not. For a lossless antenna, $\xi = 1$ and $G = D$. ◄

3-2.5 Radiation Efficiency

To a transmission line connected between a generator supplying power P_t on one end and an antenna on the other end, the antenna is merely a load with ***input impedance*** $\mathbf{Z}$. If the line is lossless and properly matched to the antenna, all of P_t is transferred to the antenna. In general, $\mathbf{Z}$ consists of a resistive component R and a reactive component X:

$$\mathbf{Z} = R + jX. \tag{3.25}$$

The resistive component is defined as equivalent to a resistor R that would consume an average power P_t when the amplitude of the ac current flowing through it is I_0,

$$P_t = \tfrac{1}{2} I_0^2 R. \tag{3.26}$$

Since $P_t = P_{rad} + P_{loss}$, it follows that R can be defined as the sum of a ***radiation resistance*** R_{rad} and a ***loss resistance*** R_{loss},

$$R = R_{rad} + R_{loss}, \tag{3.27}$$

with

$$P_{rad} = \tfrac{1}{2} I_0^2 R_{rad}, \tag{3.28a}$$

$$P_{loss} = \tfrac{1}{2} I_0^2 R_{loss}, \tag{3.28b}$$

where I_0 is the amplitude of the sinusoidal current exciting the antenna. As defined earlier, the radiation efficiency is the ratio of P_{rad} to P_t, or

$$\xi = \frac{P_{rad}}{P_t} = \frac{P_{rad}}{P_{rad} + P_{loss}} = \frac{R_{rad}}{R_{rad} + R_{loss}}. \tag{3.29}$$

The radiation resistance R_{rad} can be calculated by integrating the far-field power density over a sphere to obtain P_{rad} and then equating the result to Eq. (3.28a).

3-2.6 Effective Area of a Receiving Antenna

So far, antennas have been treated as directional radiators of energy. Now, we shall examine the reverse process, namely how a receiving antenna extracts energy from an incident wave and delivers it to a load. The ability of an antenna to capture energy from an incident wave of power density $\mathcal{S}_i$ (W/m^2) and convert it into an ***intercepted power*** P_{int} (W) for delivery to a matched load (Fig. 3-12) is characterized by the ***effective area*** A_e:

$$A_e = \frac{P_{int}}{\mathcal{S}_i} \qquad (\text{m}^2). \tag{3.30}$$

Other commonly used names for A_e include ***effective aperture*** and ***receiving cross section***. It can be

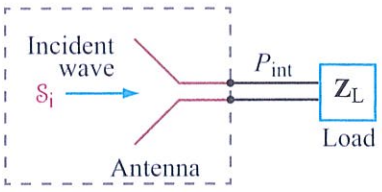

Figure 3-12: Receiving antenna represented by an equivalent circuit.

shown (Ulaby et al., 2010) that for any antenna, the directivity D, pattern solid angle Ω_p, and effective aperture A_e are related by

$$\Omega_p = \frac{\lambda^2}{A_e}, \tag{3.31a}$$

$$D = \frac{4\pi}{\Omega_p} = \frac{4\pi}{\lambda^2} A_e, \tag{3.31b}$$

which implies that a highly directional antenna (with narrow beamwidths) has a large effective area (measured in λ^2 units) and, conversely, an antenna with a broad beam has a small effective area. The concept of effective area may or may not bear a meaningful connection to the ***physical aperture*** A_p of the antenna, depending on whether or not the antenna has a definable physical aperture. For dipoles and many other wire antennas, the antenna directivity D does not depend on the wire diameter, so it is theoretically possible to make the wire diameter infinitesimally small, thereby reducing any definition of the antenna's cross-sectional area to zero, without affecting either its D or A_e.

If the antenna has a readily definable physical aperture A_p, as in the case of horn and dish antennas, it is useful to relate A_e to A_p through the ***aperture efficiency*** η_a as follows:

$$A_e = \eta_a A_p. \tag{3.32}$$

3-3 Friis Transmission Formula

The two antennas shown in Fig. 3-13 are part of a free-space communication link, with the separation between the antennas, R, being large enough for each to be in the far-field region of the other. The transmitting and receiving antennas have ***effective areas*** A_t and A_r and ***radiation efficiencies*** ξ_t and ξ_r, respectively. Our objective is to find a relationship between P_t, the power supplied to the transmitting antenna, and P_{rec}, the power delivered to the receiver. As always, we assume that both antennas are impedance-matched to their respective transmission lines. Initially, we consider the case where

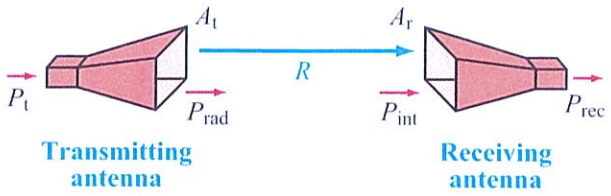

Figure 3-13: Transmitter–receiver configuration.

the two antennas are oriented such that the peak of the radiation pattern of each antenna points in the direction of the other.

We start by treating the transmitting antenna as a lossless isotropic radiator. The power density incident upon the receiving antenna at a distance R from an isotropic transmitting antenna is simply equal to the transmitter power P_t divided by the surface area of a sphere of radius R:

$$\mathcal{S}_{iso} = \frac{P_t}{4\pi R^2}. \tag{3.33}$$

The real transmitting antenna is neither lossless nor isotropic. Hence, the received power density $\mathcal{S}_r$ due to the real antenna is

$$\mathcal{S}_r = G_t \mathcal{S}_{iso} = \xi_t D_t \mathcal{S}_{iso} = \frac{\xi_t D_t P_t}{4\pi R^2}. \tag{3.34}$$

Through the gain $G_t = \xi_t D_t$, ξ_t accounts for the fact that only part of the power P_t supplied to the antenna is radiated out into space, and D_t accounts for the directivity of the transmitting antenna (in the direction of the receiving antenna). Moreover, by Eq. (3.31b), the peak directivity D_t is related to A_t by $D_t = 4\pi A_t/\lambda^2$. Hence, Eq. (3.34) becomes

$$\mathcal{S}_r = \frac{\xi_t A_t P_t}{\lambda^2 R^2}. \tag{3.35}$$

On the receiving-antenna side, the power intercepted by the receiving antenna is equal to the product of the incident power density $\mathcal{S}_r$ and the effective area A_r:

$$P_{int} = \mathcal{S}_r A_r = \frac{\xi_t A_t A_r P_t}{\lambda^2 R^2}. \tag{3.36}$$

The power delivered to the receiver, P_{rec}, is equal to the intercepted power P_{int} multiplied by the radiation efficiency of the receiving antenna, ξ_r. Hence, $P_{rec} = \xi_r P_{int}$, which leads to the result

$$\frac{P_{rec}}{P_t} = \frac{\xi_t \xi_r A_t A_r}{\lambda^2 R^2} = G_t G_r \left(\frac{\lambda}{4\pi R}\right)^2. \tag{3.37}$$

▶ This relation is known as the ***Friis transmission formula***, and P_{rec}/P_t is called the ***power transfer ratio***. ◀

If the two antennas are not oriented in the direction of maximum power transfer, Eq. (3.37) assumes the general form

$$\frac{P_{rec}}{P_t} = \left(\frac{\lambda}{4\pi R}\right)^2 G_t(\theta_t, \phi_t)\, G_r(\theta_r, \phi_r), \tag{3.38}$$

where $G_t(\theta_t, \phi_t)$ is the gain of the transmitting antenna at angles (θ_t, ϕ_t) corresponding to the direction of the receiving antenna (as seen by the antenna pattern of the transmitting antenna), and a similar definition applies to $G_r(\theta_r, \phi_r)$ for the receiving antenna.

For a pair of lossless isotropic antennas with $G_t = G_r = 1$,

$$\frac{P_{rec}}{P_t} = \left(\frac{\lambda}{4\pi R}\right)^2 = \frac{1}{L_{FS}} \quad \textbf{(lossless isotropic antennas)},$$

where $L_{FS} = (4\pi R/\lambda)^2$ is called the ***free-space propagation loss***. In terms of L_{FS}, Eq. (3.38) can be rewritten as

$$\frac{P_{rec}}{P_t} = \frac{1}{L_{FS}} G_t(\theta_t, \phi_t)\, G_r(\theta_r, \phi_r). \tag{3.39}$$

The Friis transmission formula can also be applied to calculate the power reflected by a specular surface. In Fig. 3-14(a), the transmitter and receiver are oriented along the specular direction relative to the reflecting surface ($\theta_i = \theta_r$) and their antennas have the same polarization state. Using image theory, the configuration in Fig. 3-14(a) is equivalent to that in Fig. 3-14(b). In the latter, the range between the transmitter and the receiver is $(R_1 + R_2)$. Also, reflection by the surface modifies the power density by the factor $\Gamma^p(\theta)$, the p-polarized Fresnel reflectivity (with $p = $ v or h). Incorporating these

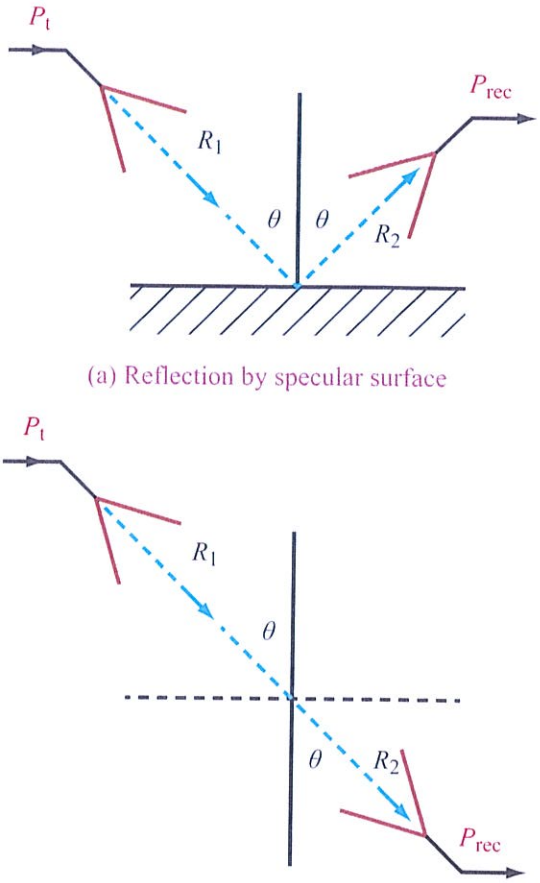

Figure 3-14: Reflection by a specular surface is equivalent to direct transmission along a path of length $(R_1 + R_2)$, but modified by the reflectivity of the surface $\Gamma^p(\theta)$.

modifications into Eq. (3.37) leads to

$$\frac{P_{\text{rec}}}{P_{\text{t}}} = G_{\text{t}}G_{\text{r}}\left[\frac{\lambda}{4\pi(R_1+R_2)}\right]^2 \Gamma^p(\theta), \quad (p = \text{h or v}). \tag{3.40}$$

3-4 Radiation by Large-Aperture Antennas

For wire antennas, the sources of radiation are the infinitesimal current elements comprising the current distribution along the wire, and the total radiated field at a given point in space is equal to the sum, or integral, of the fields radiated by all the elements. A parallel scenario applies to aperture antennas, except that now the source of radiation is the electric-field distribution across the aperture. Consider the horn antenna shown in Fig. 3-15(a). It is connected to a source through a coaxial transmission line, with the outer conductor of the line connected to the metal body of the horn and the inner conductor made to protrude, through a small hole, partially into the throat end of the horn, thereby providing a transition from coax to waveguide. The protruding conductor acts as a monopole antenna, generating waves that radiate along the short waveguide segment and then outwardly toward the horn's aperture. The electric field of the wave arriving at the aperture, which may vary as a function of x_a and y_a over the horn's aperture, is called the ***electric-field aperture distribution*** or ***illumination***, $E_a(x_a, y_a)$. Inside the horn, wave propagation is guided by the horn's geometry, but as the wave transitions from a guided wave into an unbounded wave, every point of its wavefront serves as a source of spherical secondary wavelets. The aperture may then be represented as a distribution of isotropic radiators. At a distant point Q, the combination of all the waves arriving from all of these radiators constitutes the total wave observed by a receiver placed at that point.

The radiation process described for the horn antenna is equally applicable to any aperture upon which an electromagnetic wave is incident. For example, in the case of the parabolic reflector shown in Fig. 3-15(b), it can be described in terms of an imaginary aperture representing the electric-field distribution across a plane in front of the reflector.

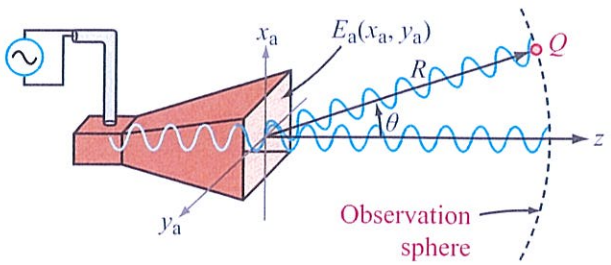

(a) A horn antenna with aperture field distribution $E_a(x_a, y_a)$

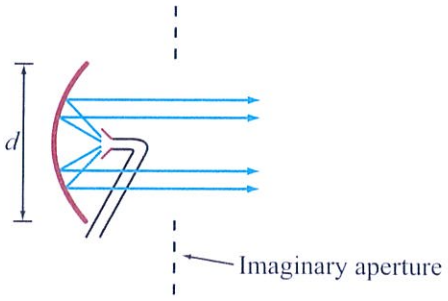

(b) Radiation by a parabolic dish reflector illuminated by a small horn antenna

Figure 3-15: (a) A horn antenna with aperture field distribution $E_a(x_a, y_a)$, and (b) radiation by a parabolic dish reflector illuminated by a small horn antenna.

Two types of mathematical formulations are available for computing the electromagnetic fields of waves radiated by apertures. The first is a ***scalar formulation*** based on Kirchhoff's work and the second is a ***vector formulation*** based on Maxwell's equations. In this section, we limit our presentation to the scalar diffraction technique, in part because of its inherent simplicity and also because it is applicable to a wide range of practical applications.

▶ The key requirement for the validity of the scalar formulation is that the antenna aperture be at least several wavelengths long along each of its principal dimensions. ◀

A distinctive feature of such an antenna is its high directivity and correspondingly narrow beam, which makes it attractive for microwave remote-sensing systems. The frequency range commonly used for such systems is the 1 to 300 GHz band. Because the corresponding wavelength range is 30 cm to 1 mm, respectively, it is quite practical to construct and use antennas (in this frequency range) with aperture dimensions that are many wavelengths in size.

The x_a–y_a plane in Fig. 3-16, denoted ***aperture plane*** A, contains an aperture with an electric field distribution $E_a(x_a, y_a)$. For the sake of convenience, the opening has been chosen to be rectangular in shape, with dimensions l_x along x_a and l_y along y_a, even though the formulation we are about to discuss is general enough to accommodate any two-dimensional aperture distribution, including those associated with circular and elliptical apertures. At a distance z from plane A in Fig. 3-16, we have an observation plane O with axes (x, y). The two planes have parallel axes and are separated by a distance z. Moreover, z is sufficiently large that any point Q in the observation plane is in the far-field region of the aperture. To satisfy the far-field condition, it is necessary that

$$R \geq 2d^2/\lambda \qquad \textbf{(far-field distance)}. \tag{3.41}$$

where, as noted earlier in connection with Eq. (3.1), d is the longest linear dimension of the radiating aperture.

The position of observation point Q is specified by the range R between the center of the aperture and point Q and by the angles θ and ϕ (Fig. 3-16), which jointly define the direction of the observation point relative to the coordinate system of the aperture. The z axis is orthogonal to the plane containing the antenna aperture. Also, θ usually is called the ***elevation angle***.

The electric field phasor of the wave incident upon point Q is denoted $E(R, \theta, \phi)$. ***Kirchhoff's scalar diffraction theory*** provides the following relationship between the radiated field $E(R, \theta, \phi)$ and the aperture illumination $E_a(x_a, y_a)$:

$$E(R, \theta, \phi) = \frac{j}{\lambda}\left(\frac{e^{-jkR}}{R}\right) h(\theta, \phi), \tag{3.42}$$

where

$$h(\theta, \phi) = \iint_{-\infty}^{\infty} E_a(x_a, y_a) \cdot \exp\left[jk \sin\theta (x_a \cos\phi + y_a \sin\phi)\right] dx_a\, dy_a, \tag{3.43}$$

where $k = 2\pi/\lambda$ is the wave number. We shall refer to $h(\theta, \phi)$ as the ***form factor*** of $E(R, \theta, \phi)$. Its integral is written with infinite limits, with the understanding that $E_a(x_a, y_a)$ is identically zero outside the aperture. The spherical propagation factor (e^{-jkR}/R) accounts for wave propagation between the center of the aperture and the observation point, and $h(\theta, \phi)$ represents an integration of the exciting field $E_a(x_a, y_a)$ over the extent of the aperture, taking into account [through the exponential function in Eq. (3.43)] the approximate deviation in distance between R and s, where s is the distance to any point (x_a, y_a) in the aperture plane (see Fig. 3-16).

▶ In Kirchhoff's scalar formulation, the polarization direction of the radiated field $E(R, \theta, \phi)$ is the same as that of the aperture field $E_a(x_a, y_a)$. ◀

The power density of the radiated wave is given by

$$\mathcal{S}(R, \theta, \phi) = \frac{|E(R, \theta, \phi)|^2}{2\eta_0} = \frac{|h(\theta, \phi)|^2}{2\eta_0 \lambda^2 R^2}. \tag{3.44}$$

3-5 Rectangular Aperture with Uniform Field Distribution

In the general case, $E_a(x_a, y_a)$ is a complex quantity consisting of an amplitude distribution and a phase distribution over the aperture. As we will see in future

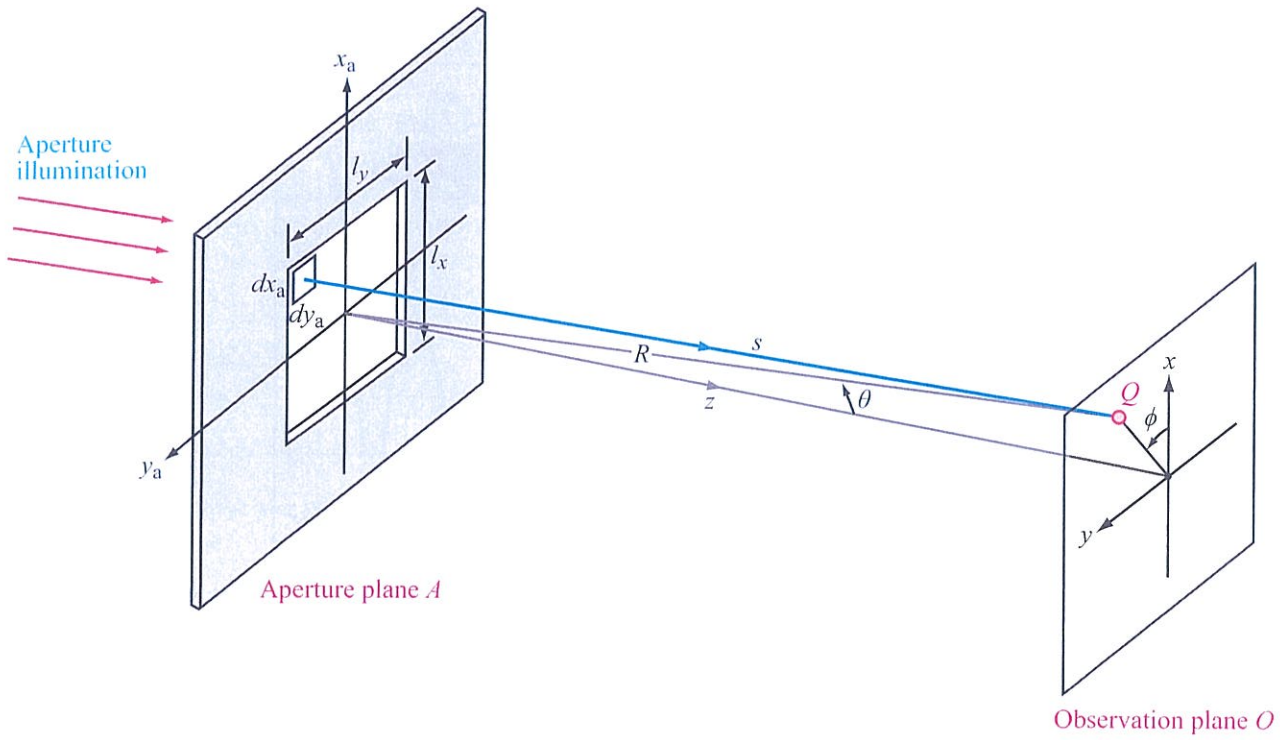

Figure 3-16: Radiation by an aperture in the x_a–y_a plane at $z = 0$.

sections, the two distributions govern both the shape and direction of the antenna pattern.

To illustrate the scalar diffraction technique, consider a rectangular aperture of height l_x and width l_y, both at least a few wavelengths long. The aperture is excited by a ***uniform field distribution*** (i.e., constant value) given by

$$E_a(x_a, y_a) = \begin{cases} E_0 & \text{for } -l_x/2 \le x_a \le l_x/2 \\ & \text{and } -l_y/2 \le y_a \le l_y/2, \\ 0 & \text{otherwise.} \end{cases} \quad (3.45)$$

Inserting Eq. (3.45) into Eq. (3.43) gives

$$h(\theta,\phi) = \int_{y_a=-l_y/2}^{l_y/2} \int_{x_a=-l_x/2}^{l_x/2} E_0 \exp[jk \sin\theta \cos\phi\, x_a] \cdot \exp[jk \sin\theta \sin\phi\, x_a]\, dx_a\, dy_a. \quad (3.46)$$

In preparation for performing the integration, we introduce the intermediate variables u and v defined as

$$u = k \sin\theta \cos\phi = \frac{2\pi}{\lambda} \sin\theta \cos\phi, \quad (3.47a)$$

$$v = k \sin\theta \sin\phi = \frac{2\pi}{\lambda} \sin\theta \sin\phi. \quad (3.47b)$$

Use of Eq. (3.47) in Eq. (3.46) leads to

$$h(\theta,\phi) = E_0 \int_{-l_x/2}^{l_x/2} e^{jux_a}\, dx_a \int_{-l_y/2}^{l_y/2} e^{jvy_a}\, dy_a. \quad (3.48)$$

After performing the integration in Eq. (3.48), replacing u and v with the expressions given in Eq. (3.47), and finally inserting the expression for $h(\theta,\phi)$ into

Eq. (3.42), we obtain the result

$$E(R,\theta,\phi) = \frac{jE_0A_p}{\lambda}\left(\frac{e^{-jkR}}{R}\right)\text{sinc}\left(\frac{\pi l_x}{\lambda}\sin\theta\cos\phi\right) \cdot \text{sinc}\left(\frac{\pi l_y}{\lambda}\sin\theta\sin\phi\right), \quad (3.49)$$

where $A_p = l_x l_y$ and the sinc function for any argument t is defined as[†]

$$\text{sinc}\, t = \frac{\sin t}{t}. \quad (3.50)$$

3-5.1 Antenna Pattern in x–y Plane

To illustrate the result represented by Eq. (3.49), let us examine the x–z elevation pattern of the antenna at a fixed range **R**. Setting $\phi = 0$ in Eq. (3.49) and then using Eq. (3.44) leads to

$$\mathcal{S}(R,\theta) = \mathcal{S}_0\,\text{sinc}^2(\pi l_x \sin\theta/\lambda) \quad (x\text{–}z \text{ plane}), \quad (3.51)$$

where $\mathcal{S}_0 = E_0^2A_p^2/(2\eta_0\lambda^2R^2)$.

> ► The sinc function is maximum when its argument is zero; i.e., sinc(0) = 1. ◄

This occurs when $\theta = 0$. Hence, at a fixed range R, $\mathcal{S}_{max} = \mathcal{S}(\theta{=}0) = \mathcal{S}_0$. The normalized radiation intensity is then given by

$$F(\theta) = \frac{\mathcal{S}(R,\theta)}{\mathcal{S}_{max}} = \text{sinc}^2\left(\frac{\pi l_x}{\lambda}\sin\theta\right) = \text{sinc}^2(\pi\gamma) \quad (x\text{–}z \text{ plane}). \quad (3.52)$$

Figure 3-17 shows $F(\theta)$ plotted (on a decibel scale) as a function of the intermediate variable $\gamma = (l_x/\lambda)\sin\theta$. The pattern exhibits nulls at nonzero integer values of γ.

[†]This is one of two common definitions for the sinc function; the other is $\text{sinc}\, t = \sin(\pi t)/(\pi t)$. In this chapter we use the definition given by Eq. (3.50) exclusively.

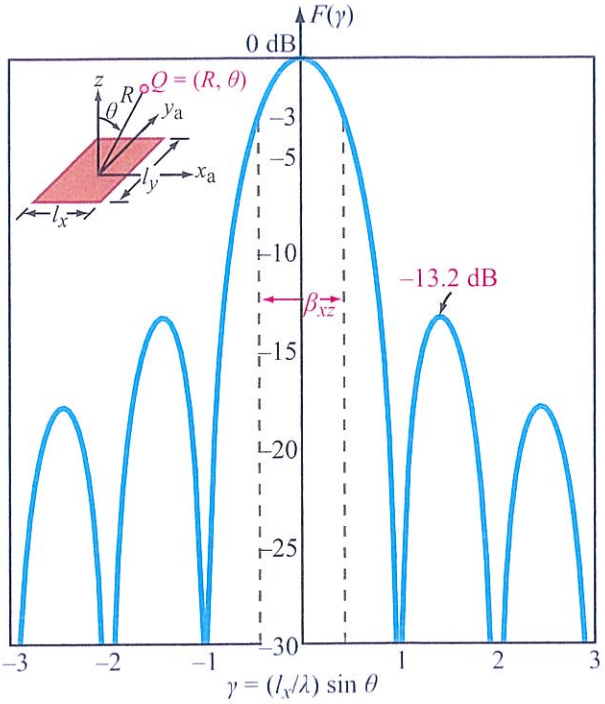

Figure 3-17: Normalized radiation pattern of a uniformly illuminated rectangular aperture in the x–z plane ($\phi = 0$).

3-5.2 Beamwidth

The normalized radiation intensity $F(\theta)$ is symmetrical in the x–z plane, and its maximum is along the boresight direction ($\theta = 0$ in this case). Its half-power beamwidth $\beta_{xz} = \theta_2 - \theta_1$, where θ_1 and θ_2 are the values of θ at which $F(\theta,0) = 0.5$ (or -3 dB on a decibel scale), as shown in Fig. 3-17. Since the pattern is symmetrical with respect to $\theta = 0$, $\theta_1 = -\theta_2$ and $\beta_{xz} = 2\theta_2$. The angle θ_2 can be obtained from a solution of

$$F(\theta_2) = \text{sinc}^2\left(\frac{\pi l_x}{\lambda}\sin\theta_2\right) = 0.5. \quad (3.53)$$

Solution of Eq. (3.53) yields the result

$$\frac{\pi l_x}{\lambda}\sin\theta_2 = 1.39, \quad (3.54)$$

or

$$\sin\theta_2 = 0.44\,\frac{\lambda}{l_x}\,. \qquad (3.55)$$

A fundamental condition for the validity of scalar diffraction theory is that the aperture dimensions are much larger than the wavelength λ; that is, $\lambda/l_x \ll 1$. Hence, θ_2 is a small angle, the approximation $\sin\theta_2 \approx \theta_2$ is appropriate, and the half-power beamwidth of a rectangular aperture is

$$\beta_{xz} = 2\theta_2 \approx 2\sin\theta_2 = 0.88\frac{\lambda}{l_x} \quad \text{(rad)}. \qquad (3.56a)$$

A similar solution for the y–z plane ($\phi = \pi/2$) gives

$$\beta_{yz} = 0.88\,\frac{\lambda}{l_y} \quad \text{(rad)}. \qquad (3.56b)$$

▶ The uniform aperture distribution ($E_a = E_0$ across the aperture) gives a far-field pattern with the narrowest possible beamwidth. ◀

The first sidelobe level is 13.2 dB below the peak value (see Fig. 3-17), which is equivalent to 4.8% of the peak value. If the intended application calls for a pattern with a lower sidelobe level (to avoid interference with signals from sources along directions outside the main beam of the antenna pattern), this can be accomplished by using a ***tapered aperture distribution*** (Sections 3-7 and 3-8), one in which the electric field intensity is weighted over the aperture with a maximum at the center and decreases toward the edges.

▶ A tapered distribution provides a pattern with lower sidelobes, but the mainlobe becomes wider. ◀

As discussed later in Section 3-7, the steeper the taper, the lower are the sidelobes and the wider is the mainlobe. In general, the beamwidth in a given plane, say the x–z plane, is given by

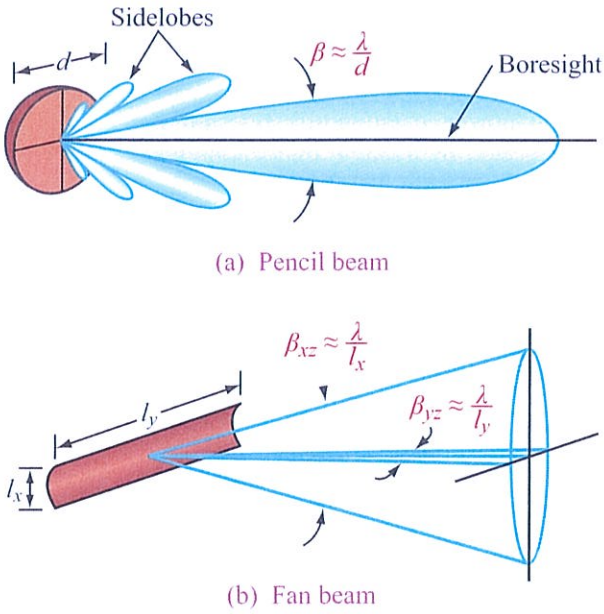

Figure 3-18: Radiation patterns of (a) a circular reflector and (b) a cylindrical reflector (sidelobes not shown).

$$\beta_{xz} = k_x\frac{\lambda}{l_x}\,, \qquad (3.57)$$

where k_x is a constant related to the steepness of the taper. For a uniform distribution with no taper, $k_x = 0.88$, whereas for a highly tapered distribution, $k_x \approx 2$. In the typical case, $k_x \approx 1$.

To illustrate the relationship between the antenna dimensions and the corresponding beam shape, we show in Fig. 3-18 the radiation patterns of a circular reflector and a cylindrical reflector. The circular reflector has a circularly symmetric pattern, whereas the pattern of the cylindrical reflector has a narrow beam in the azimuth plane corresponding to its long dimension and a wide beam in the elevation plane corresponding to its narrow dimension. For a circularly symmetric antenna pattern, the beamwidth β is related to the diameter d by the approximate relation $\beta \approx \lambda/d$.

3-5.3 Directivity and Effective Area

In Section 3-2.3, we derived an approximate expression [Eq. (3.21)] for the antenna directivity D in terms of the half-power beamwidths β_{xz} and β_{yz} for antennas characterized by a single major lobe whose boresight is along the z direction:

$$D \approx \frac{4\pi}{\beta_{xz}\beta_{yz}} . \tag{3.58}$$

If we use the approximate relations $\beta_{xz} \approx \lambda/l_x$ and $\beta_{yz} \approx \lambda/l_y$, we obtain

$$D \approx \frac{4\pi l_x l_y}{\lambda^2} = \frac{4\pi A_p}{\lambda^2} . \tag{3.59}$$

More precisely, for any antenna, its directivity is related to its effective area A_e by Eq. (3.31b):

$$D = \frac{4\pi A_e}{\lambda^2} . \tag{3.60}$$

▶ As a first-order approximation, the effective area of an aperture antenna is equal to its physical aperture; that is, $A_e \approx A_p$. ◀

To compute D accurately, it is necessary to execute the following steps:

1. For a specified aperture distribution $E_a(x_a, y_a)$, use Eqs. (3.42) and (3.43) to determine the radiated field $E(R, \theta, \phi)$.
2. Compute power density $\mathcal{S}(R, \theta, \phi) = |E|^2/2\eta_0$, and then determine the direction at which $\mathcal{S}$ is at its maximum value (at a fixed R). Call it $\mathcal{S}_{max}$.
3. Obtain the normalized radiation intensity

$$F(\theta, \phi) = \left. \frac{\mathcal{S}(R, \theta, \phi)}{\mathcal{S}_{max}} \right|_{@ \text{ same } R} .$$

4. Use Eq. (3.18) to compute D.
5. Use Eq. (3.31b) to compute the effective area A_e.
6. The aperture efficiency is then given by $\xi_a = A_e/A_p$, where A_p is the physical aperture of the antenna.

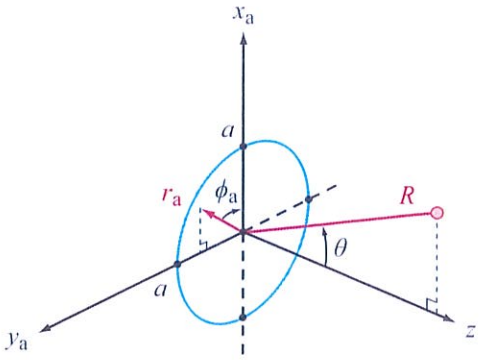

(a) Circular aperture in the x_a-y_a plane

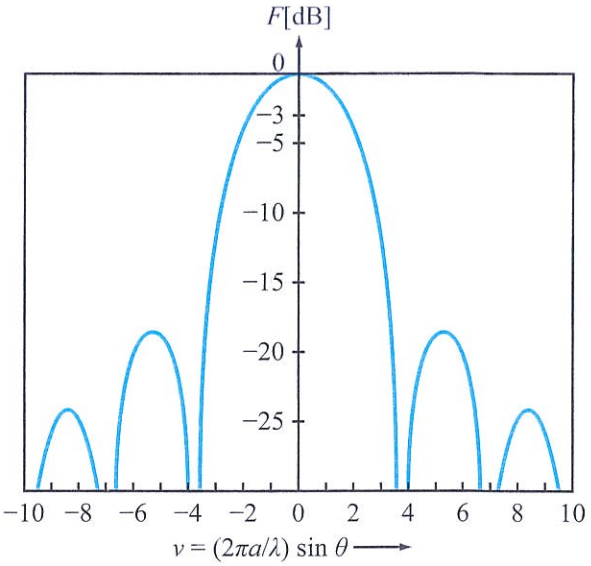

(b) Radiation pattern

Figure 3-19: Circular aperture and its radiation pattern.

3-6 Circular Aperture with Uniform Field Illumination

For circularly symmetric aperture illuminations, the far-field patterns can be found most conveniently if we first express x_a and y_a in terms of the polar coordinates r_a and ϕ_a (Fig. 3-19a) as follows:

$$x_a = r_a \cos\phi_a, \tag{3.61a}$$

$$y_a = r_a \sin\phi_a. \tag{3.61b}$$

Substituting the above equations in Eq. (3.43) and replacing the elemental area $dx_a\, dy_a$ with its polar-coordinate equivalent $r_a\, dr_a\, d\phi_a$, the form factor $h(\theta,\phi)$ becomes

$$h(\theta,\phi) = \int_0^{2\pi}\int_0^{\infty} E_a(r_a) \times \exp[jkr_a \sin\theta(\cos\phi\cos\phi_a + \sin\phi\sin\phi_a)] r_a\, dr_a\, d\phi_a, \tag{3.62}$$

or equivalently,

$$h(\theta,\phi) = \int_0^{2\pi}\int_0^{\infty} E_a(r_a) \times \exp[jkr_a \sin\theta\cos(\phi-\phi_a)] r_a\, dr_a\, d\phi_a. \tag{3.63}$$

Using the Bessel-function identity

$$J_0(x) = \frac{1}{2\pi}\int_0^{2\pi} \exp[jx\cos(\phi-\phi_a)]\, d\phi_a,$$

where J_0 is a zero-order Bessel function of the first kind, the expression given by Eq. (3.63) can be simplified to:

$$h(\theta,\phi) = h(\theta) = 2\pi\int_0^{\infty} E_a(r_a)\, J_0(kr_a \sin\theta)\, r_a\, dr_a. \tag{3.64}$$

Note that because of the circular symmetry, the dependence on the angles ϕ and ϕ_a has disappeared. Evaluation of Eq. (3.64) as a function of θ leads to the radiation pattern shown in Fig. 3-19(b), plotted as a function of the variable $v = (2\pi a/\lambda)\sin\theta$. The width of the mainlobe between first nulls can be shown to be

$$\beta_{\text{null}} = 2[\sin^{-1}(0.61\lambda/a)] \approx 1.22\lambda/a = 2.44\lambda/d, \tag{3.65}$$

where $d = 2a$ is the aperture diameter.

In a similar fashion, the half-power beamwidth can be obtained by setting $F(v) = 0.5$, which leads to $v = 1.57$ and

$$\beta_{1/2} = 2[\sin^{-1}(0.25\lambda/a)] \approx 0.5\lambda/a = \lambda/d. \tag{3.66}$$

Following the same procedure used earlier in connection with the rectangular aperture, the maximum directivity of the circular aperture can be shown to be

$$D = \frac{4\pi A_p}{\lambda^2}, \tag{3.67}$$

and in terms of $\beta_{1/2}$,

$$D = 0.78\,\frac{4\pi}{\beta_{1/2}^2}. \tag{3.68}$$

3-7 Nonuniform-Amplitude Illumination

By controlling the shape of the amplitude illumination, the antenna designer can optimize certain features of interest such as the antenna directivity, the sidelobe level, or the location of the nulls in the radiation pattern. Since these features are interrelated, the optimization process is determined by the intended application.

To illustrate the influence of the amplitude illumination on the far-field pattern of a rectangular aperture, we consider some commonly used distributions. For simplicity, we limit our discussion to the x–z plane ($\phi = 0$), uniform-phase illumination, and unity-amplitude illumination in the y_a direction. That is, we define $E_a(x_a, y_a)$ as a product of ***separable distributions***,

$$E_a(x_a, y_a) = E_1(x_a)\, E_2(y_a), \tag{3.69}$$

and then we set $E_2(y_a) = 1$.

Introducing the new variables

$$x_1 = \frac{2}{l_x}x_a, \tag{3.70a}$$

$$u_1 = \frac{\pi l_x}{\lambda}\sin\theta, \tag{3.70b}$$

the form factor $h(\theta,\phi)$ given by Eq. (3.43) becomes

$$h(\theta) = \frac{l_x l_y}{2}\int_{x_1=-1}^{1} E_1(x_1)\, e^{ju_1 x_1}\, dx_1 \qquad (at\ \phi = 0). \tag{3.71}$$

Table 3-1: Radiation patterns produced by various types of amplitude distributions along x_1 over a rectangular aperture $l_x \times l_y$.

Amplitude distribution[a]		Relative directivity[b]	Sidelobe level (dB)[c]	Half-power (−3 dB) beamwidth (radians)[d]
Cosine: $E_1(x_1) = \cos^n(\pi x_1/2)$				
	$n = 0$[e]	1.00	13.2	$0.88\lambda/l_x$
	$n = 1$	0.81	23	$1.20\lambda/l_x$
	2	0.67	32	$1.45\lambda/l_x$
	3	0.58	40	$1.66\lambda/l_x$
	4	0.52	48	$1.94\lambda/l_x$
Parabolic: $E_1(x_1) = 1 - (1 - \Delta)x_1^2$				
	$\Delta = 1.0$[e]	1.00	13.2	$0.88\lambda/l_x$
	0.8	0.99	15.8	$0.92\lambda/l_x$
	0.5	0.97	17.1	$0.97\lambda/l_x$
	0	0.83	20.6	$1.15\lambda/l_x$
Triangular: $E_1(x_1) = 1 - \lvert x_1 \rvert$		0.75	26.4	$1.28\lambda/l_x$

[a]The variable $x_1 = (2/l_x)x_a$, and $|x_1| \leq 1$. [b]Relative to a uniform aperture distribution. [c]Below maximum intensity. [d]In x–z plane. [e]Same as uniform-distribution case.

Antenna radiation performance usually is described in terms of its normalized radiation intensity $F(\theta)$, which is proportional to $|h(\theta)|^2$.

Table 3-1 provides a summary of three important characteristics of $|h(u_1)|^2$ for several classes of amplitude illumination $E_1(x_1)$. These characteristics are the directivity D relative to the uniform illumination case, the sidelobe level in dB below peak intensity, and the half-power beamwidth $\beta_{1/2}$. Complete expressions for $h(u_1)$ for these and other illuminations are available in the literature (Silver, 1949; Hansen, 1964).

For the first class of illumination in Table 3-1, $E_1(x_1) = \cos^n(\pi x_1/2)$, the illumination decreases from 1.0 at the center of the aperture ($x_1 = 0$) to zero at the edges ($x_1 = \pm 1$) for $n > 1$. As n increases, faster roll-off illumination tapers are produced, resulting in lower sidelobe levels, at the expense, however, of lower directivities and wider beamwidths. This is true also for the second class of illumination included in Table 3-1

Table 3-2: Radiation patterns produced by the amplitude distribution function $E(r_1) = (1 - r_1^2)^n$ over a circular aperture of diameter d.

n	Relative directivity[a]	Sidelobe level (dB)[b]	Half-power (−3 dB) beamwidth (radians)
0 (uniform)	1.00	17.6	$1.02\lambda/d$
1	0.75	24.6	$1.27\lambda/d$
2	0.55	30.6	$1.47\lambda/d$
3	0.45	36.1	$1.65\lambda/d$

The variable $r_1 = (2/d)r_a$ and $0 \le r_1 \le 1$. [a]Relative to a uniform aperture distribution. [b]Below maximum intensity.

as well as for the illumination given in Table 3-2 for circular apertures.

Note that for the amplitude distributions listed in Table 3-1, the taper occurs along x_a only. If an identical taper occurs along y_a as well, the radiation pattern exhibits similar first sidelobe levels and half power beamwidths in the y–z plane (with $\beta_{1/2}$ being inversely proportional to l_y), and the relative directivity becomes the squared value of the value listed in Table 3-1. For example, if $E_a(x_a, y_a)$ has a cosine taper with $n = 1$ along both x_a and y_a, the relative directivity becomes $(0.81)^2 = 0.66$. Also, the effective aperture becomes approximately

$$A_e \approx \frac{\lambda^2}{\beta_{xz}\beta_{yz}} = \frac{\lambda^2}{(1.2\lambda/\lambda_x)(1.2\lambda/\lambda_y)} \approx 0.69 l_x l_y = 0.69 A_p.$$

3-8 Beam Efficiency

Consider a square aperture with $l_x = l_y = l$ situated in the x_a–y_a plane. The aperture dimension l is at least several wavelengths long; consequently, the radiation pattern is highly directional and has a narrow mainlobe. Figure 3-20 displays plots of the radiation pattern in the x–z plane for two types of aperture illuminations, a uniform illumination and a cosine distribution with $n = 1$ (see Table 3-1). In each case, the same illumination is applied along aperture axis x_a as along y_a. Hence, the radiation patterns are the same in the x–z and y–z planes.

The uniform-illumination radiation pattern, labeled $F_u(\gamma)$ in Fig. 3-20, is an exact replica of the pattern shown earlier in Fig. 3-17. Its half-power beamwidth is $\beta_u = \beta_{xz} = \beta_{yz} = 0.88\lambda/l$. If $l = 10\lambda$, $\beta_u = 0.088$ rad $\approx 5°$. The first sidelobe is 13.2 dB below the maximum value of $F_u(\gamma)$, corresponding to a level of only 4.8%, which means that the power radiated by such an antenna along the direction corresponding to the peak of the first sidelobe is less than 5% of that radiated along the main-beam axis. This may be quite adequate for many applications, but not for microwave radiometry.

The radiation pattern labeled $F_c(\gamma)$ in Fig. 3-20 corresponds to a cosine-tapered illumination with $n = 1$ along both x_a and y_a. Its half-power beamwidth is $\beta_c = 1.2\lambda/l$, which is 36% wider than that of the

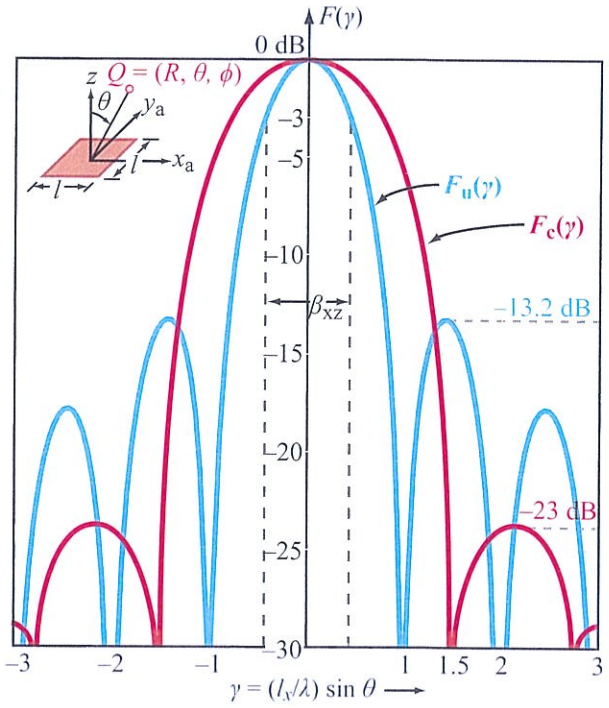

Figure 3-20: Comparison of the antenna pattern $F_u(\gamma)$ of a uniformly illuminated aperture with $F_c(\gamma)$ for a cosine-tapered illuminated aperture.

uniformly illuminated aperture, but its first sidelobe is at 23 dB below the peak (or 0.5%), which is 10 times better than that of the uniformly illuminated aperture. Lowering the sidelobes is equivalent to "squeezing" their pattern content into the mainlobe, causing it to become wider.

For an antenna with radiation pattern $F(\theta,\phi)$, the ***beam efficiency*** η_b is defined as

$$\eta_b = \frac{\text{power radiated in cone with half-angle } \theta_l}{\text{total power radiated in } 4\pi \text{ sr}} = \frac{\int_0^{2\pi}\int_0^{\theta_l} F(\theta,\phi)\sin\theta\, d\theta\, d\phi}{\int_0^{2\pi}\int_0^{\pi} F(\theta,\phi)\sin\theta\, d\theta\, d\phi} = \frac{\Omega_m}{\Omega_p}, \quad (3.72)$$

where Ω_m and Ω_p are the ***main-beam solid angle*** and ***pattern solid angle***, respectively, and angle θ_l is selected such that the cone encompassed within it is a good approximation of the mainlobe of the antenna pattern. Typically, θ_l is defined as the angle between the beam axis and the first minimum.

For $F_u(\gamma)$ in Fig. 3-20, θ_l corresponds to $\gamma_l = 1$, and since $\sin\theta \approx \theta$, it follows that

$$\theta_{l_u} = \frac{\lambda}{l} \quad \textbf{(uniform illumination)}. \quad (3.73a)$$

The first null of the tapered-illumination radiation pattern occurs at $\gamma_l = 1.5$. Hence,

$$\theta_{l_c} = 1.5\,\frac{\lambda}{l}. \quad (3.73b)$$

(cosine illumination with $n = 1$)

To illustrate with an example, let us consider a uniformly illuminated square antenna with $l = 10\lambda$. Computing Eq. (3.72) with $\theta_l = 0.1$ rad and

$$F(\theta,\phi) = \text{sinc}^2\left(\frac{\pi l_x}{\lambda}\sin\theta\cos\phi\right)\text{sinc}^2\left(\frac{\pi l_y}{\lambda}\sin\theta\sin\phi\right) = \text{sinc}^2(10\pi\sin\theta\cos\phi)\,\text{sinc}^2(10\pi\sin\theta\sin\phi), \quad (3.74)$$

leads to $\eta_b \approx 0.8$, or 80%. This means that 80% of the total power radiated by the antenna is radiated along directions within the mainlobe, and the remaining 20% is lost to other directions. Conversely, if the antenna is operating in a receiving mode and power is incident upon it uniformly from all directions, 20% of the total power it receives comes in from directions outside the mainlobe.

A similar evaluation carried out for the cosine-tapered illumination with $n = 1$ leads to a beam efficiency $\eta_b \approx 93\%$, and for $n = 2$, $\eta_b \approx 98\%$.

► The application of steep illumination tapers can raise the beam efficiency to $\approx 100\%$, at the expense of a wider mainlobe and a smaller directivity. ◄

Nevertheless, as we discuss later in Chapter 6, high beam efficiency is critically important for making accurate measurements with a microwave radiometer.

3-9 Antenna Arrays

► When two or more antennas are used together, the combination is called an ***antenna array***. ◄

Even though an array need not consist of similar radiating elements, most arrays actually use identical elements, such as dipoles, slots, horn antennas, or parabolic dishes. The antenna elements of an array may be arranged in various configurations, but the most common are the linear one-dimensional configuration—wherein the elements are arranged along a straight line—and the two-dimensional lattice configuration in which the elements sit on a planar grid. The desired shape of the far-field radiation pattern of the array can be synthesized by controlling the relative amplitudes of the array elements' excitations.

► Through the use of electronically controlled solid-state phase shifters, the beam direction of the antenna array can be steered electronically by controlling the relative phases of the array elements. ◄

This flexibility of the array antenna has led to numerous applications, including ***electronic steering*** and ***multiple-beam generation***.

The purpose of this and the next two sections is to introduce the reader to the basic principles of array theory and design techniques used in shaping the antenna pattern and steering the mainlobe. The presentation is confined to the one-dimensional linear array with equal spacing between adjacent elements.

A linear array of N identical radiators is arranged along the z axis as shown in Fig. 3-21. The radiators are fed by a common oscillator through a branching network. In each branch, an attenuator (or amplifier) and phase shifter are inserted in series to control the amplitude and phase of the signal feeding the antenna element in that branch.

In the far-field region of any radiating element, the ***element electric-field intensity*** $E_e(R,\theta,\phi)$ may be expressed as a product of two functions: the spherical propagation factor e^{-jkR}/R, which accounts for the dependence on the range R, and $f_e(\theta,\phi)$, which accounts for the directional dependence of the element's electric field. Thus, for an isolated element, the radiated field is

$$E_e(R,\theta,\phi) = \frac{e^{-jkR}}{R} f_e(\theta,\phi), \tag{3.75}$$

and the corresponding power density $\mathcal{S}_e$ is

$$\mathcal{S}_e(R,\theta,\phi) = \frac{1}{2\eta_0}|E_e(R,\theta,\phi)|^2 = \frac{1}{2\eta_0 R^2}|f_e(\theta,\phi)|^2. \tag{3.76}$$

For the array shown in Fig. 3-21(b), the far-zone field due to element i at observation point Q at range R_i is

$$E_i(R_i,\theta,\phi) = A_i \frac{e^{-jkR_i}}{R_i} f_e(\theta,\phi), \tag{3.77}$$

where $A_i = a_i e^{j\psi_i}$ is a ***complex feeding coefficient*** representing the amplitude a_i and phase ψ_i of the excitation giving rise to E_i, relative to the phase of a reference excitation. In practice, the excitation of one of the elements is used as reference. Note that R_i and A_i may be different for different elements in the array, but $f_e(\theta,\phi)$ is the same for all of the antenna elements because they are identical, and hence exhibit identical directional patterns.

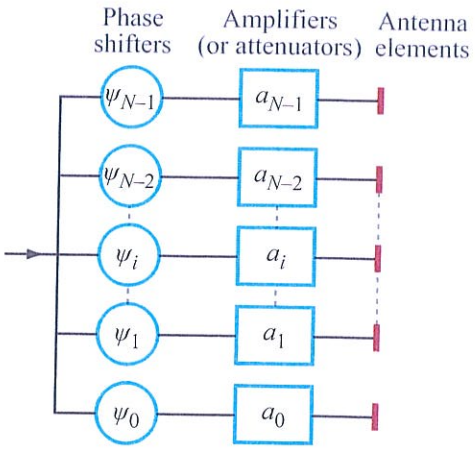

(a) Array elements with individual amplitude and phase control

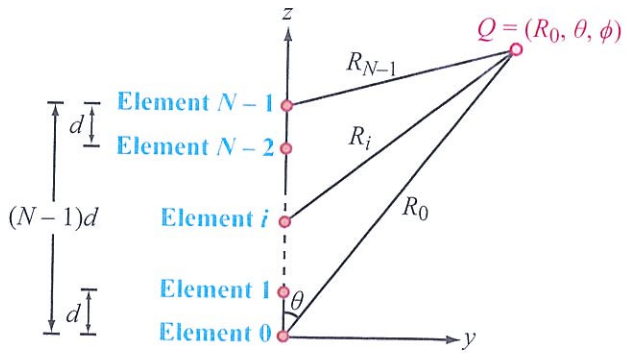

(b) Array geometry relative to observation point

Figure 3-21: Linear-array configuration and geometry.

The total field at the observation point $Q(R_0, \theta, \phi)$ is the sum of the fields due to the N elements:

$$E(R_0,\theta,\phi) = \sum_{i=0}^{N-1} E_i(R_i,\theta,\phi)$$

$$= \left[\sum_{i=0}^{N-1} A_i \frac{e^{-jkR_i}}{R_i}\right] f_e(\theta,\phi), \qquad (3.78)$$

where R_0 denotes the range of Q from the center of the coordinate system, chosen to be at the location of the zeroth element. To satisfy the far-field condition given by Eq. (3.41) for an array of length $l = (N-1)d$, where d is the interelement spacing, the range R_0 should be sufficiently large to satisfy

$$R_0 \geq \frac{2l^2}{\lambda} = \frac{2(N-1)^2 d^2}{\lambda}. \qquad (3.79)$$

This condition allows us to ignore differences in the distances from Q to the individual elements as far as the magnitudes of the radiated fields are concerned. Thus, we can set $R_i = R_0$ in the denominator in Eq. (3.78) for all i. With regard to the phase part of the propagation factor, we can use the parallel-ray approximation given by

$$R_i \approx R_0 - z_i \cos\theta = R_0 - id\cos\theta, \qquad (3.80)$$

where $z_i = id$ is the distance between the ith element and the zeroth element (Fig. 3-22). Employing these two approximations in Eq. (3.78) leads to

$$E(R_0,\theta,\phi) = f_e(\theta,\phi)\left(\frac{e^{-jkR_0}}{R_0}\right)\left[\sum_{i=0}^{N-1} A_i e^{jikd\cos\theta}\right], \qquad (3.81)$$

and the corresponding array-antenna power density is given by

$$\mathcal{S}(R_0,\theta,\phi) = \frac{1}{2\eta_0}|E(R_0,\theta,\phi)|^2$$

$$= \frac{1}{2\eta_0 R_0^2}|f_e(\theta,\phi)|^2 \left|\sum_{i=0}^{N-1} A_i e^{jikd\cos\theta}\right|^2.$$

Use of Eq. (3.76) leads to

$$\mathcal{S}(R_0,\theta,\phi) = \mathcal{S}_e(R_0,\theta,\phi)\left|\sum_{i=0}^{N-1} A_i e^{jikd\cos\theta}\right|^2. \qquad (3.82)$$

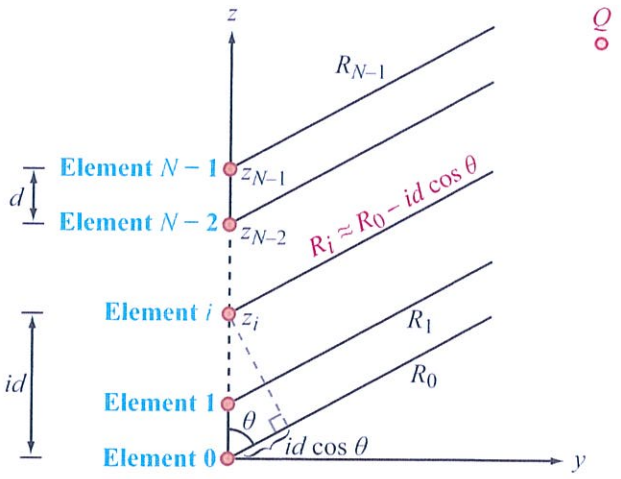

Figure 3-22: The rays between the elements and a far-away observation point are approximately parallel lines. Hence, the distance $R_i \approx R_0 - id\cos\theta$.

This expression is a product of two factors. The first factor, $\mathcal{S}_e(R_0,\theta,\phi)$, is the power density of the energy radiated by an individual element, and the second, called the ***array factor***, is a function of the positions of the individual elements and their feeding coefficients, but not a function of the specific type of radiator used.

> ▶ The array factor represents the far-field radiation intensity of the N elements, had the elements been isotropic radiators. ◀

Denoting the ***array factor*** by

$$F_a(\theta) = \left|\sum_{i=0}^{N-1} A_i e^{jikd\cos\theta}\right|^2, \qquad (3.83)$$

the power density of the antenna array is then written as

$$\mathcal{S}(R_0,\theta,\phi) = \mathcal{S}_e(R_0,\theta,\phi)\, F_a(\theta). \qquad (3.84)$$

This equation demonstrates the ***pattern multiplication principle***. It allows us to find the far-field power density

of the antenna array by first computing the far-field power pattern with the array elements replaced with isotropic radiators, which yields the array factor $F_a(\theta)$, and then multiplying the result by $\mathcal{S}_e(R_0,\theta,\phi)$, the power density for a single element (which is the same for all elements).

The feeding coefficient A_i is, in general, a complex amplitude consisting of an amplitude factor a_i and a phase factor ψ_i:

$$A_i = a_i e^{j\psi_i}. \tag{3.85}$$

Insertion of Eq. (3.85) into Eq. (3.83) leads to

$$F_a(\theta) = \left|\sum_{i=0}^{N-1} a_i e^{j\psi_i} e^{jikd\cos\theta}\right|^2. \dagger \tag{3.86}$$

The array factor is governed by two input functions: the ***array amplitude distribution*** given by the a_i's and the ***array phase distribution*** given by the ψ_i's. The amplitude distribution serves to control the shape of the array radiation pattern, while the phase distribution can be used to steer its direction.

3-10 N-Element Array with Uniform Phase Distribution

We now consider an array of N elements with equal spacing d and equal-phase excitations; that is, $\psi_i = \psi_0$ for $i = 1,2,\ldots,(N-1)$. Such an array of ***in-phase elements*** is sometimes referred to as a ***broadside array*** because the main beam of the radiation pattern of its array factor is always in the direction broadside to the array axis. From Eq. (3.86), the array factor is given by

$$\begin{aligned} F_a(\theta) &= \left|e^{j\psi_0}\sum_{i=0}^{N-1} a_i e^{jikd\cos\theta}\right|^2 \\ &= |e^{j\psi_0}|^2\left|\sum_{i=0}^{N-1} a_i e^{jikd\cos\theta}\right|^2 = \left|\sum_{i=0}^{N-1} a_i e^{jikd\cos\theta}\right|^2. \end{aligned} \tag{3.87}$$

†Computer Code 3.1.

The phase difference between the fields radiated by adjacent elements is

$$\gamma = kd\cos\theta = \frac{2\pi d}{\lambda}\cos\theta. \tag{3.88}$$

In terms of γ, Eq. (3.87) takes the compact form

$$F_a(\gamma) = \left|\sum_{i=0}^{N-1} a_i e^{ji\gamma}\right|^2 \quad \textbf{(uniform phase)}. \tag{3.89}$$

3-10.1 Uniform Amplitude Distribution

For a uniform amplitude distribution with $a_i = 1$ for $i = 0,1,\ldots,(N-1)$, Eq. (3.89) becomes

$$F_a(\gamma) = |1 + e^{j\gamma} + e^{j2\gamma} + \cdots + e^{j(N-1)\gamma}|^2. \tag{3.90}$$

This geometric series can be rewritten (Ulaby et al., 2010) in the compact form

$$F_a(\gamma) = |f_a(\gamma)|^2, \tag{3.91}$$

with

$$f_a(\gamma) = e^{j(N-1)\gamma/2}\,\frac{\sin(N\gamma/2)}{\sin(\gamma/2)}. \tag{3.92}$$

After multiplying $f_a(\gamma)$ by its complex conjugate, we obtain the following result for the array factor:

$$F_a(\gamma) = \frac{\sin^2(N\gamma/2)}{\sin^2(\gamma/2)}. \tag{3.93}$$

(uniform amplitude and phase)

From Eq. (3.90), $F_a(\gamma)$ is maximum when all terms are 1, which occurs when $\gamma = 0$ (or equivalently, $\theta = \pi/2$). Moreover, $F_a(0) = N^2$. Hence, the normalized array factor is given by

$$\begin{aligned} F_{an}(\gamma) &= \frac{F_a(\gamma)}{F_{a,max}} = \frac{\sin^2(N\gamma/2)}{N^2\sin^2(\gamma/2)} \\ &= \frac{\sin^2\left(\dfrac{N\pi d}{\lambda}\cos\theta\right)}{N^2\sin^2\left(\dfrac{\pi d}{\lambda}\cos\theta\right)}. \end{aligned} \tag{3.94}$$

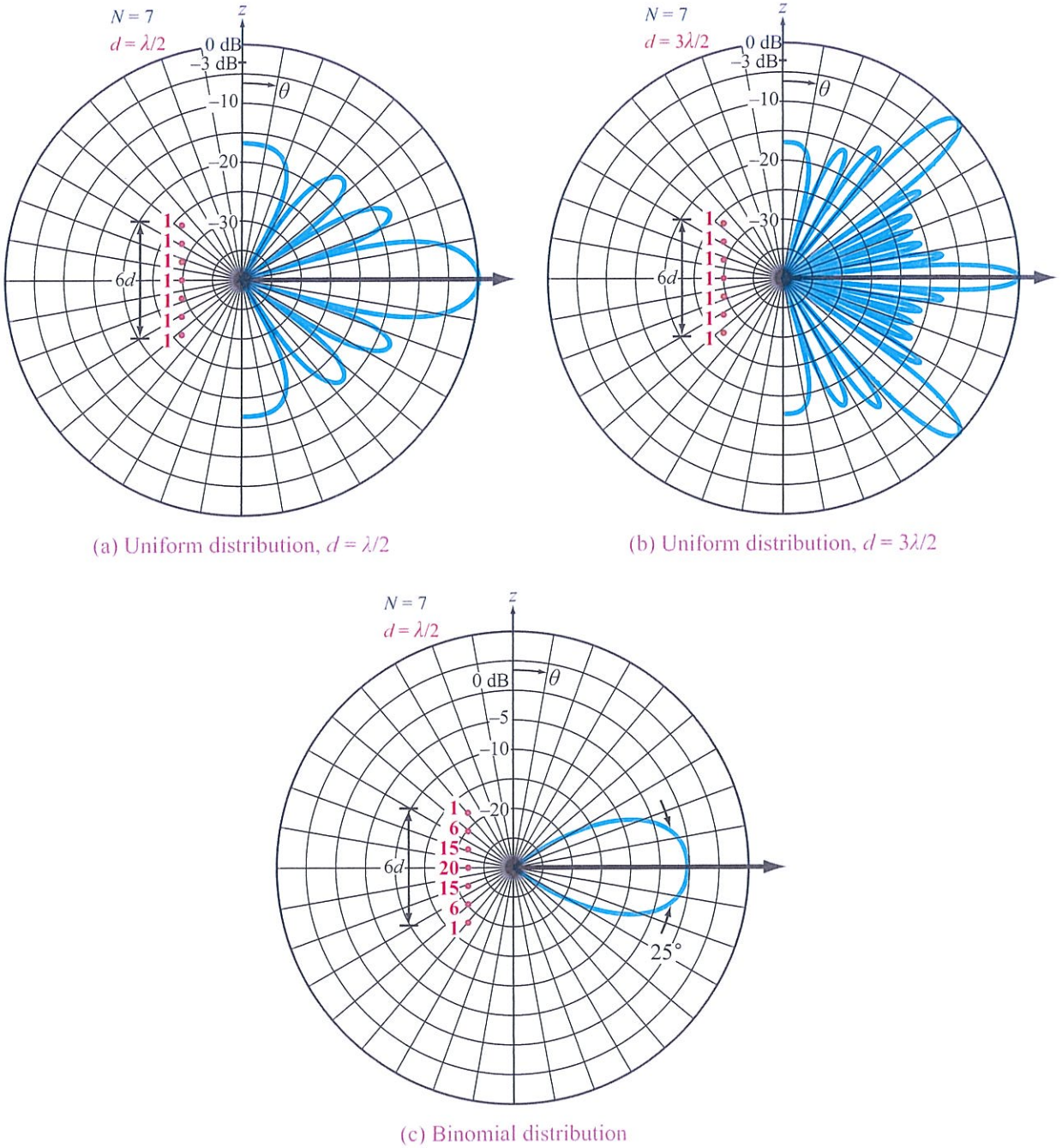

Figure 3-23: Normalized array patterns of 7-element arrays: (a) uniform distribution with $d = \lambda/2$, (b) uniform distribution with $d = 3\lambda/2$, and (c) binomial distribution with $d = \lambda/2$.

A polar plot of $F_{an}(\theta)$ is shown in Fig. 3-23(a) for $N = 7$ and $d = \lambda/2$. The reader is reminded that this is a plot of the radiation pattern of the array factor alone; the pattern for the antenna array is equal to the product of this pattern and that of a single element, as discussed earlier in connection with the pattern multiplication principle.

3-10.2 Grating Lobes

Even though Eq. (3.94) is defined for all values of γ, only the interval $0 \le \theta \le \pi$ pertains to the real antenna situation. This interval is called the ***visible*** region of the antenna array. The array pattern shown in Fig. 3-23(a) for the uniform array with $d = \lambda/2$ consists of a single pattern, whereas if the interelement spacing is increased to $d = 3\lambda/2$, the pattern gets repeated three times, as shown in Fig. 3-23(b). The multiple patterns, called ***grating lobes***, are introduced by the repetitive behavior of the sine function in the denominator of Eq. (3.94). The grating lobes are spaced 2π apart along the γ axis. To avoid grating lobes, it is necessary that

$$|\gamma| = \left| \left(\frac{2\pi d}{\lambda} \right) \cos\theta \right| \le 2\pi.$$

Over the visible region, $0 \le \theta \le \pi$, the above inequality is satisfied if $d \le \lambda$. For $d = \lambda$, two grating lobes exist, one on each side of the mainlobe, with their peaks (of the same amplitude as that of the mainlobe) pointing along the two directions of the array axis. Since the radiation pattern of the array antenna is the product of the array factor and the radiation pattern of an individual element, grating lobes may be unimportant if the element pattern has small values (relative to its peak value) in those directions. *When phase delay is introduced between adjacent array elements at their inputs in order to steer the antenna beam into a direction other than broadside (Section 3-11), avoiding grating lobes requires that $d \le \lambda/2$.* This condition is analogous to the Nyquist sampling theorem in communication theory (Ulaby and Yagle, 2013).

3-10.3 Binomial Distribution

In some applications, it may be preferable to have a less directive array factor than that of the uniform array, but with lower sidelobe levels. To reduce sidelobe levels, several nonuniform amplitude distributions have been proposed. Among these is the ***binomial distribution***, so designated because the a_i's, the amplitudes of array elements, are proportional to the binomial coefficients:

$$a_i = \frac{(N-1)!}{i!(N-i-1)!}$$

with $i = 0, 1, \ldots, N-1$. To illustrate with an example, the relative amplitudes of a seven-element binomial array are $a_0 = a_6 = 1$, $a_1 = a_5 = 6$, $a_2 = a_4 = 15$, and $a_3 = 20$. With these coefficients, the array factor defined by Eq. (3.89) becomes

$$F_a(\gamma) = \left| 1 + 6e^{j\gamma} + 15e^{j2\gamma} + 20e^{j3\gamma} + 15e^{j4\gamma} + 6e^{j5\gamma} + e^{j6\gamma} \right|^2. \quad (3.95)$$

Transferring the array phase reference from the edge to the center by factoring out $e^{j3\gamma}$, the array factor can be expressed in terms of cosine functions of γ:

$$\begin{aligned} F_a(\gamma) &= \left| e^{j3\gamma}(e^{-j3\gamma} + 6e^{-j2\gamma} + 15e^{-j\gamma} + 20 + 15e^{j\gamma} + 6e^{j2\gamma} + e^{j3\gamma}) \right|^2 \\ &= (20 + 30\cos\gamma + 12\cos 2\gamma + 2\cos 3\gamma)^2. \end{aligned}$$

The pattern maximum occurs at $\gamma = 0$, and the corresponding peak value is $F_a(0) = (64)^2 = 4096$. The normalized array factor, $F_{an}(\gamma) = F_a(\gamma)/F_a(0)$, is shown in Fig. 3-23(c) for $d = \lambda/2$. The binomial array exhibits no minor lobes, but its half-power beamwidth is substantially larger than that of the uniform array.

3-11 Electronic Scanning of Arrays

The discussion in the preceding section was concerned with uniform-phase arrays, in which the phases of the feeding coefficients, ψ_0 to ψ_{N-1}, are all equal. In this section, we examine the use of phase delay between adjacent elements as a tool to ***electronically steer*** the direction of the array-antenna beam from broadside at $\theta = 90°$ to any desired angle θ_0. By eliminating the need to mechanically steer an antenna to change its beam's

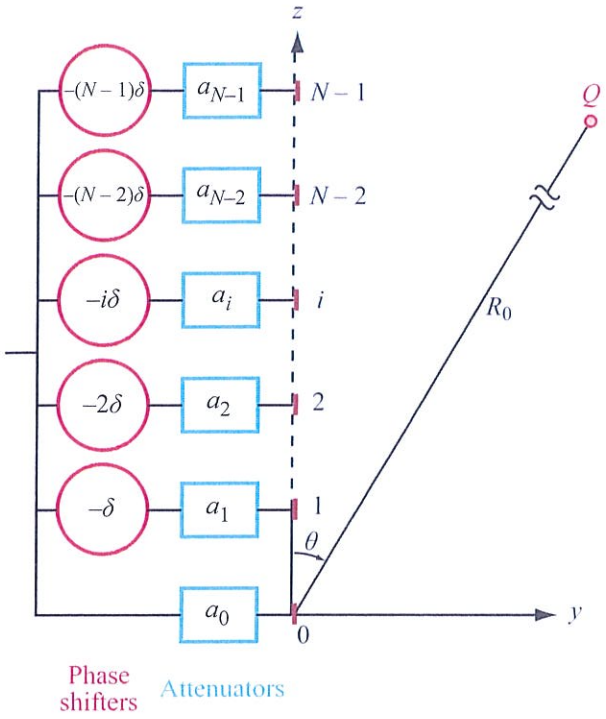

Figure 3-24: The application of linear phase.

direction, electronic steering allows beam scanning at very fast rates.

► Electronic steering is achieved by applying a ***linear phase distribution*** across the array: $\psi_0 = 0$, $\psi_1 = -\delta$, $\psi_2 = -2\delta$, etc. ◄

As shown in Fig. 3-24, the phase of the ith element, relative to that of the zeroth element, is

$$\psi_i = -i\delta, \tag{3.96}$$

where δ is the ***incremental phase delay*** between adjacent elements. Use of Eq. (3.96) in Eq. (3.86) leads to

$$\begin{aligned} F_a(\theta) &= \left| \sum_{i=0}^{N-1} a_i e^{-ji\delta} e^{jikd\cos\theta} \right|^2 \\ &= \left| \sum_{i=0}^{N-1} a_i e^{ji(kd\cos\theta - \delta)} \right|^2 \\ &= \left| \sum_{i=0}^{N-1} a_i e^{ji\gamma'} \right|^2 = F_a(\gamma'),^{\dagger} \end{aligned} \tag{3.97}$$

where we introduced a new variable given by

$$\gamma' = kd\cos\theta - \delta. \tag{3.98}$$

For reasons that become clear later, we define the phase shift δ in terms of an angle θ_0, which we call the ***scan angle***, as follows:

$$\delta = kd\cos\theta_0. \tag{3.99}$$

Hence, γ' becomes

$$\gamma' = kd(\cos\theta - \cos\theta_0). \tag{3.100}$$

The array factor given by Eq. (3.97) has the same functional form as the array factor developed earlier for the uniform-phase array [see Eq. (3.89)], except that γ is replaced with γ'. Hence:

► For any amplitude distribution across an array, the array factor $F_a(\gamma')$ when excited by a linear-phase distribution can be obtained from $F_a(\gamma)$, the expression developed for the array assuming a uniform-phase distribution, by replacing γ with γ'. ◄

If the amplitude distribution is symmetrical with respect to the array center, the array factor $F_a(\gamma')$ is maximum when its argument $\gamma' = 0$. When the phase is uniform ($\delta = 0$), this condition corresponds to the direction

[†] **Computer Code 3.2.**

$\theta = 90°$, which is why the uniform-phase arrangement is called a broadside array. According to Eq. (3.100), in a linearly phased array, $\gamma' = 0$ when $\theta = \theta_0$. Thus, by applying linear phase across the array, the array pattern is shifted along the $\cos\theta$ axis by an amount $\cos\theta_0$, and the direction of maximum radiation is ***steered*** from the broadside direction ($\theta = 90°$) to the direction $\theta = \theta_0$. To steer the beam all the way to the ***end-fire direction*** ($\theta = 0$), the incremental phase shift δ should be equal to kd radians.

To illustrate the process with an example, consider the case of the N-element array excited by a uniform-amplitude distribution. Its normalized array factor is given by Eq. (3.94). Upon replacing γ with γ', we have

$$F_{an}(\gamma') = \frac{\sin^2(N\gamma'/2)}{N^2 \sin^2(\gamma'/2)}, \qquad (3.101)$$

with γ' as defined by Eq. (3.100). For an array with $N = 10$ and $d = \lambda/2$, plots of the mainlobe of $F_{an}(\theta)$ are shown in Fig. 3-25 for $\theta_0 = 0°$, 45°, and 90°. We note that the half-power beamwidth increases as the array beam is steered from broadside to end fire.

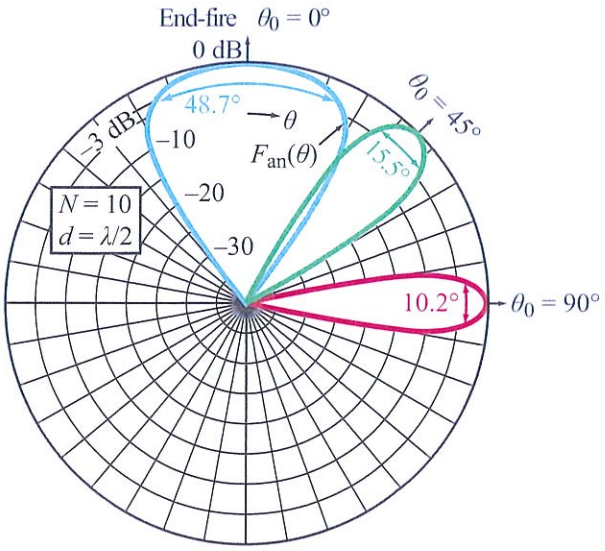

Figure 3-25: Normalized array pattern of a 10-element array with $\lambda/2$ spacing between adjacent elements. All elements are excited with equal amplitude. Through the application of linear phase across the array, the main beam can be steered from the broadside direction ($\theta_0 = 90°$) to any scan angle θ_0. Equiphase excitation corresponds to $\theta_0 = 90°$.

3-12 Antenna Types

Antennas are constructed in a wide variety of geometrical configurations and feeding arrangements. A specific antenna type usually is chosen on the basis of its radiation pattern, gain, polarization, impedance, and bandwidth. In some applications, geometry also may be important. For example, the antenna used for a side-looking airborne radar (SLAR) needs to be long in the direction of flight (so as to produce a narrow beam in the along-track direction) and narrow in height (so as to illuminate a wide swathwidth on the ground). Although both the waveguide slot array antenna and the cylindrical reflector antenna fed by a dipole array can provide the desired illumination pattern, the waveguide slot array or microstrip patch array (Section 3-12.3) are more suitable aerodynamically.

A thorough treatment of the various types of antennas used in microwave remote sensing would constitute a sizable volume in itself. Therefore, we have chosen to consider below two basic types of antennas—the electromagnetic horn and the slot antenna—as examples with which to illustrate how the techniques discussed in previous sections may be applied to determine their radiation properties. More detailed treatments of these and other types of antennas, including reflector, log-periodic, and lens antennas, are contained in the books and handbooks listed at the end of the book.

3-12.1 Horn Antennas

Electromagnetic horns are widely used in microwave communication and remote-sensing systems. Small horns with modest gain are used commonly as primary antennas to illuminate ("feed") large apertures such as reflector-type antennas, while large horns with high gain are employed on their own in some applications.

The horn antenna provides a gradual transition between a waveguide and free space. If the waveguide

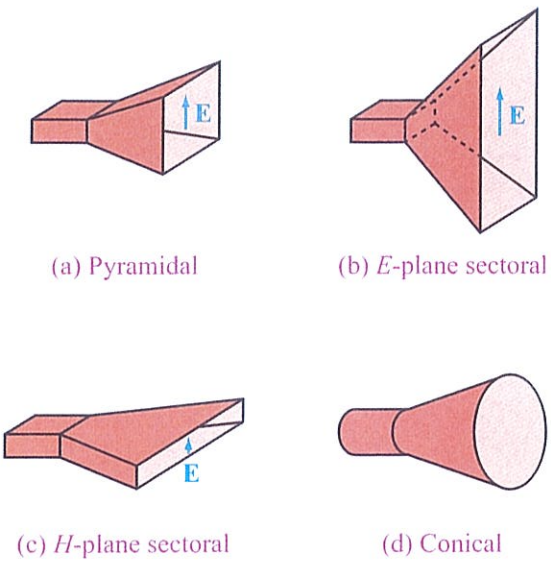

(a) Pyramidal (b) *E*-plane sectoral

(c) *H*-plane sectoral (d) Conical

Figure 3-26: Commonly used types of horn antennas.

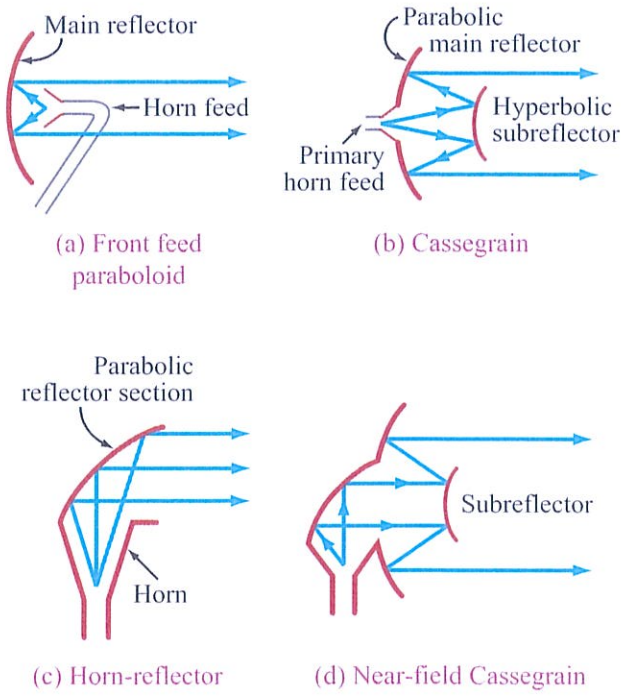

(a) Front feed paraboloid (b) Cassegrain

(c) Horn-reflector (d) Near-field Cassegrain

Figure 3-27: Horn-reflector antennas.

dimensions are such that it can support only the dominant propagation mode, then by gradually flaring the terminal section of the waveguide, the excitation of higher-order modes may be avoided. Thus, a horn can provide simultaneously single-mode propagation (which is difficult to achieve with an oversize open-ended waveguide) as well as a large radiating aperture (compared to the single-mode waveguide). Furthermore, horns are broader-band antennas than dipole and slot antennas.

Horns are constructed in a variety of shapes; some of the more frequently used types are illustrated in Fig. 3-26. The combination of size and shape of a horn dictates its directivity, impedance, shape of radiation pattern, and polarization properties. The horn shown in Fig. 3-26(a) is known as a ***pyramidal horn***. It is often called a "standard-gain horn" because it is commonly used in antenna measurements as a reference antenna of known gain. A pyramidal horn flared in only one plane is known as a ***sectoral horn***. If the waveguide is flared to increase the aperture dimension in the direction of the electric field [Fig. 3-26(b)], it is referred to as an ***E-plane sectoral horn***, and if the flaring is in the direction of the magnetic field, it is an ***H-plane sectoral horn*** [Fig. 3-26(c)]. In the nonflared direction, the sectoral horn usually has the same dimension as the waveguide connected to its throat. Another horn configuration is the ***conical horn*** [Fig. 3-26(d)], which, by virtue of its axial symmetry, produces a symmetrical radiation pattern. Horn antennas also have been combined with reflector antennas in a variety of different configurations, some of which are illustrated in Fig. 3-27.

Rectangular horns

Expressions for the radiation from open-ended waveguides and horns of rectangular aperture were derived by Barrow and Chu (1939) and Chu (1940), and are given by Risser (in Silver, 1949). They used Maxwell's equations in spherical coordinates to solve for the field at the aperture and then applied the theory of vector diffraction to compute the far-zone field. An equivalent approach using cylindrical coordinates is available in

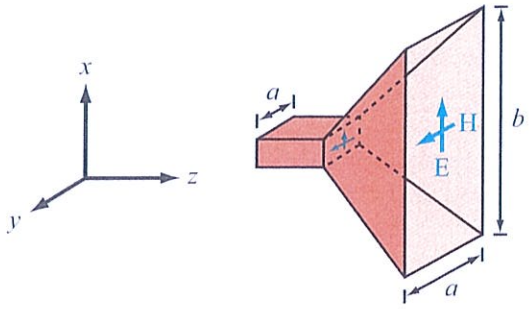

(a) Geometry

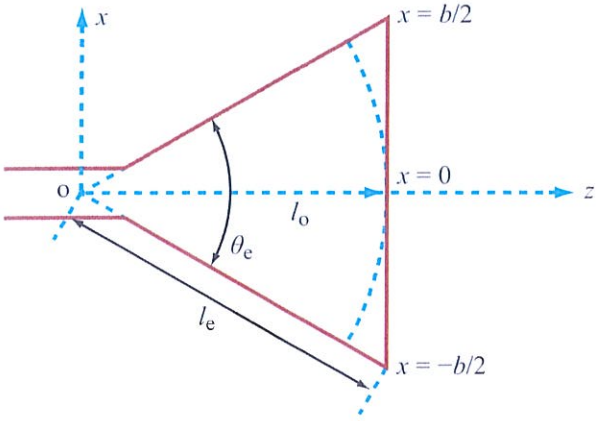

(b) x-z Plane cross section

Figure 3-28: E-plane sectoral horn geometry and coordinates.

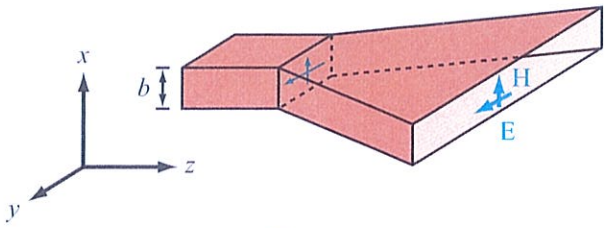

(a) Geometry

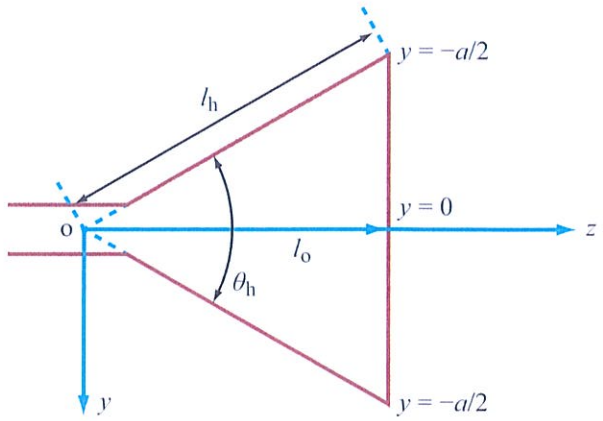

(b) y-z Plane cross section

Figure 3-29: H-plane sectoral horn geometry and coordinates.

Compton and Collin (1969a). The resultant expressions are fairly involved; hence, they are not reproduced in this presentation. Instead, we devote the remainder of this section to discussions of directivity as a function of horn dimensions.

The geometry of the E-plane sectoral horn is shown in Fig. 3-28. The angle θ_e is called the ***flare angle***, and l_e is the ***slant length***. A similar geometry applies to the H-plane sectoral horn, as shown in Fig. 3-29.

The directivity D of rectangular horns, including the pyramidal horn and the E-plane and H-plane sectoral horns, was computed by Schelkunoff (1943) for the TE_{10} mode on the basis of simplified theoretical calculations using a scalar formulation approach. Despite its theoretical simplicity, Schelkunoff's derivations provide results that have been found to be quite accurate in practice (Jakes, 1951).

E-plane sectoral horns

Schelkunoff's expression for the directivity of an E-plane horn is given by

$$D_e = \frac{64 a l_e}{\pi \lambda b} \left[C^2(\tau) + S^2(\tau) \right], \qquad (3.102)$$

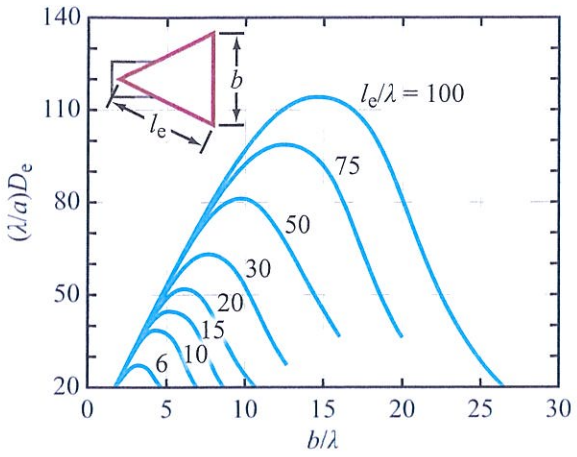

Figure 3-30: Directivity of E-plane sectoral horns with aperture height b and width a (based on Fig. 16.4 of Schelkunoff and Friis, 1952).

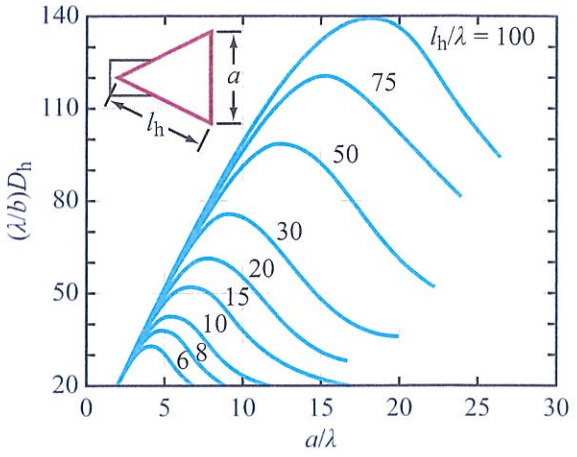

Figure 3-31: Directivity of H-plane horns of width a and height b (based on Fig. 16.3 of Schelkunoff and Friis, 1952).

where a, b, and l_e are as defined in Fig. 3-28, and C and S are the ***Fresnel integrals*** given by

$$C(\tau) = \int_0^\tau \cos\left(\frac{\pi t^2}{2}\right) dt, \tag{3.103a}$$

$$S(\tau) = \int_0^\tau \sin\left(\frac{\pi t^2}{2}\right) dt, \tag{3.103b}$$

with

$$\tau = \frac{b}{\sqrt{2\lambda l_e}}. \tag{3.103c}$$

Plots of D_e as a function of b/λ are shown in Fig. 3-30 for several values of the slant length ℓ_e. Note that for a given slant length, the directivity increases with the aperture height b until it reaches a maximum value, and then beyond this optimum aperture height the directivity decreases. This behavior is due to the nonuniform phase distribution across the aperture.

For a given value of l_e, the horn is said to be optimum if b is chosen so that the directivity D_e is maximum. This occurs when $l_e - l_0 = \lambda/4$ (Jakes, 1961). Under this condition, b and l_e are related by

$$b \approx \sqrt{2l_e\lambda}. \tag{3.104}$$

In the E plane (x–z plane in Fig. 3-28), $\beta_{1/2} \approx \lambda/b$ radians and $\beta_{\text{null}} \approx 2\lambda/b$ for the optimum E-plane sectoral horn.

H-plane sectoral horns

The directivity D_h of the H-plane horn as given by Schelkunoff (1943) is

$$D_h = \frac{4\pi b s_h}{\lambda a}\{[C(u) - C(v)]^2 + [S(u) - S(v)]^2\}, \tag{3.105}$$

where

$$u = \frac{1}{\sqrt{2}}\left(\frac{\sqrt{\lambda l_h}}{a} + \frac{a}{\sqrt{\lambda l_h}}\right), \tag{3.106a}$$

$$v = \frac{1}{\sqrt{2}}\left(\frac{a}{\sqrt{\lambda l_h}} - \frac{\sqrt{\lambda l_h}}{a}\right). \tag{3.106b}$$

Plots of D_h as a function of a/λ are shown in Fig. 3-31 for several values of the slant length l_h. The curves are similar to those of Fig. 3-30 for the E-plane horn. The H-plane sectoral horn of Fig. 3-29 is optimum when $l_h - l_0 = 3\lambda/8$, which leads to the approximate relation (Jakes, 1961)

$$a \approx \sqrt{3l_h\lambda}. \tag{3.107}$$

Pyramidal horns

The E-plane and H-plane sectoral horns have narrow beams in the flared direction and wide beams in the unflared direction. Such a beam is sometimes called a fan beam. If the application calls for narrow beams in both directions, the horn can be flared along both axes, in which case we have a pyramidal horn. Thus, a pyramidal horn may be regarded as a superposition of an E-plane and an H-plane sectoral horn.

The directivity of the pyramidal horn, D_p (Schelkunoff, 1943), may be expressed in terms of the directivities D_e and D_h as follows:

$$D_p = \frac{\pi\lambda^2}{32ab} D_e D_h, \tag{3.108}$$

where D_e and D_h are given by Eq. (3.102) and Eq. (3.105), respectively. That is, D_p may be obtained by multiplying the product of the normalized directivities $(\lambda/a)D_e$ and $(\lambda/b)D_h$ obtained from Figs. 3-30 and 3-31 by the factor $(\pi/32)$.

Conical horns

A conical horn [Fig. 3-26(d)] usually is connected to a circular waveguide excited with a TE_{11} mode. Its performance is similar to that of the pyramidal horn in that, for a fixed length, its directivity increases as a function of the aperture diameter d up to a certain optimum value. This is demonstrated in Fig. 3-32, which contains theoretical curves that were derived by Gray and Schelkunoff and reported by King (1950). Note that the family of curves is for different values of the ***axial length*** l_0, unlike the plots in Figs. 3-30 and 3-31, where the parameter was the slant length. Experimental measurements made over a wide range of values of l_0 and d were found to be in excellent agreement with the calculated values. The dashed line of Fig. 3-32 describes the dimensions of the optimum horn. The conical horn is optimum (maximum directivity for a fixed slant length l_c) when its diameter is (Jakes, 1961)

$$d \approx \sqrt{3l_c\lambda}\,, \tag{3.109}$$

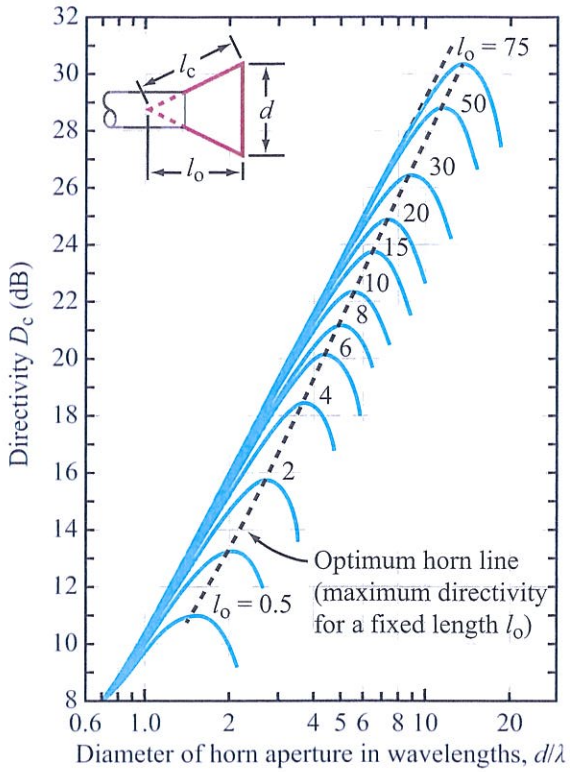

Figure 3-32: The directivity of a conical horn as a function of axial length and aperture diameter.

which is the same criterion as for the H-plane sectoral horn. Under this condition, the directivity in dB is given by

$$D_c\ [\text{dB}] = 20\log\left(\frac{\pi d}{\lambda}\right) - 2.82\ \text{dB}, \tag{3.110}$$

(optimum horn)

and its effective area is equal to 52 percent of its physical aperture area: $A_e = 0.52A_p$, where $A_p = \pi d^2/4$.

Lens-corrected horns

According to Eqs. (3.109) and (3.110), an optimum horn with a 26 dB directivity should have a slant length $l_c \approx 26\lambda$ and a diameter $d \approx 8.8\lambda$. If $\lambda = 3$ cm

($f = 10$ GHz), for example, these dimensions translate into a 78 cm long horn with an aperture diameter of 26.4 cm. For many applications, such long lengths are undesirable. If l_c were to be limited to a certain value, so would d and the directivity D_c. Because of the quadratic phase error in the aperture, increasing the aperture diameter (by increasing the flare angle) beyond its optimum value results in a loss in directivity, rather than gain. This limitation on the maximum flare angle for a given horn length has led to the development of the ***lens-corrected horn***.

By mounting a lens in the horn aperture (Fig. 3-33) to correct the phase distribution across the aperture, the limitation on the maximum flare angle can be removed, thereby allowing the use of large apertures to increase the directivity. This technique has been implemented successfully in both rectangular and conical horns. Without the lens, the phase shift between the vertex 0 and the point $x = x_1$ on the aperture (Fig. 3-33) is larger than it is to the point $x = 0$ (cone axis) because of the longer travel time. Through proper design of the lens shape and its index of refraction, the total phase shift between 0 and x_1 can be made equal to the phase-shift between 0 and the point $x = 0$ for any value of x_1 on the aperture. Effectively, the wave propagating along the cone axis has to traverse a longer thickness of the lens (in which the velocity of propagation is lower than that in air) than the wave traveling to x_1, thereby arriving in phase at the aperture.

Since the index of refraction of the lens is different from that of air, only part of the energy incident upon it is transmitted into the lens, and the remainder is reflected. Multiple reflections from the surface of the lens and the surface of the cone can result in amplitude and phase variations across the aperture. To reduce these reflections, several techniques have been developed (Compton and Collin, 1969a). The wave impedance of the lens can be matched to that of free space by covering the lens surface with a dielectric layer of appropriate thickness and index of refraction, or by cutting slots of appropriate thickness and depth into the surface of the lens (Collin, 1959).

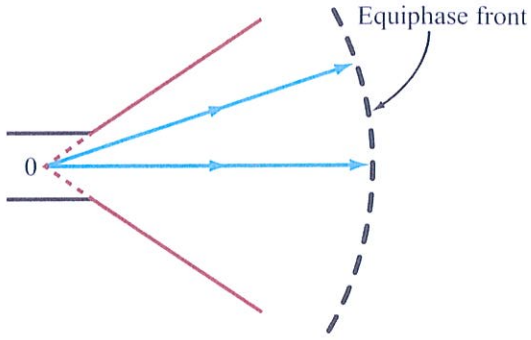

(a) Empty sectoral horn

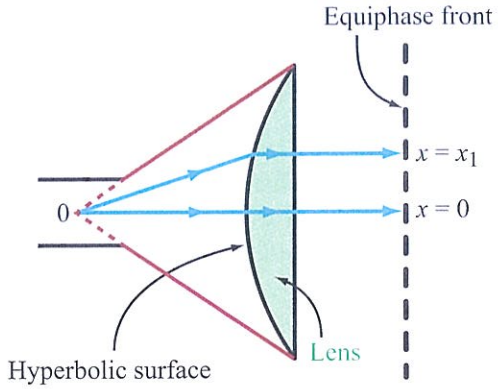

(b) Lens-corrected sectoral horn

Figure 3-33: A hyperbolic lens of the appropriate index of refraction can transform the phase front to a uniform distribution across the aperture.

3-12.2 Slot Antennas

In this section we consider the far-field radiation properties of a rectangular slot antenna, followed by a brief discussion of waveguide slot arrays.

Examples of slots cut into the walls of a rectangular waveguide are shown in Fig. 3-34. When a slot interrupts the flow of transverse surface currents, it couples energy from the waveguide to free space. Figure 3-35 shows the distribution of currents flowing along the inner walls of a rectangular waveguide propagating a

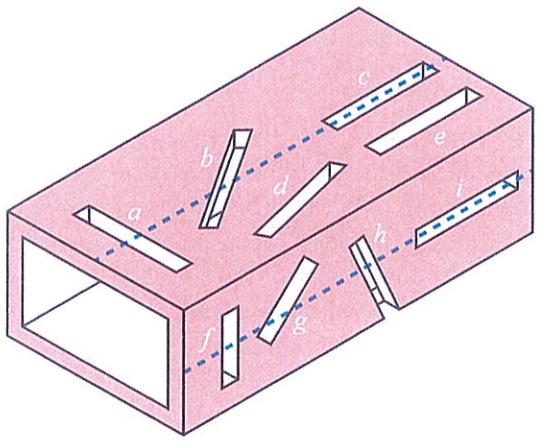

Figure 3-34: Various types of slots cut in the walls of a rectangular waveguide. Slots c and f do not radiate, because they do not interrupt the flow of surface current (see Fig. 3-35).

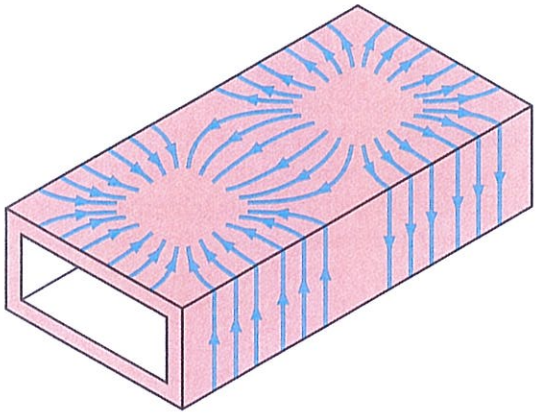

Figure 3-35: The flow of surface currents in the walls of a rectangular waveguide excited with a TE_{10} mode.

TE_{10} mode. Among the slots shown in Fig. 3-34, the only nonradiating slots are those labeled c and f (their axes are parallel to the direction of current-flaw). The magnitude of the energy coupled by a slot is a function of the waveguide dimensions; the slot dimensions, orientation, and position; and the density of the current interrupted by the slot.

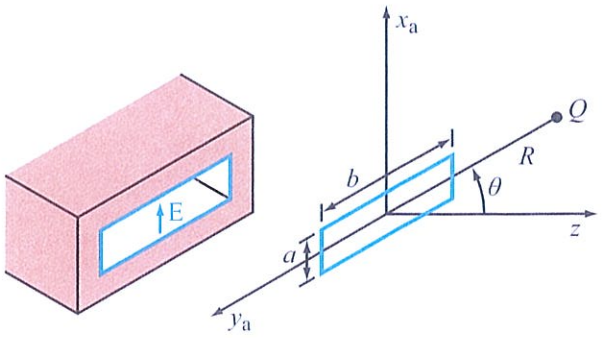

Figure 3-36: Rectangular slot with a tangential electric field in the $\hat{\mathbf{x}}_a$ direction.

To demonstrate the approach used for computing the far-zone fields of a slot antenna, we consider the simple case of a half-wave rectangular slot excited by an aperture electric field that is orthogonal to the slot axis, as shown in Fig. 3-36. More complicated configurations are beyond the scope of this presentation and are not discussed here; the interested reader is referred to Compton and Collin (1969b).

Half-wave slot

In reference to the coordinate system shown in Fig. 3-36, the tangential electric field in the aperture plane is zero everywhere except in the region of the slot. If $b = \lambda/2$ and $a \ll \lambda$, the slot behaves like a half-wave dipole with a singular beam centered along the z axis.

Waveguide slot array

We now extend the theory of linear arrays and the techniques used to provide shaped beams and electronic scanning to an array of slot radiators cut in one of the walls of a rectangular waveguide.

The choice of the geometrical configuration of the slotted waveguide array is dictated in part by the desire to minimize mutual coupling between the individual slots. Mutual coupling can influence the radiation properties of the slots as well as change their input impedance, thereby causing reflections toward the feed structure, which in turn modify the amplitude and

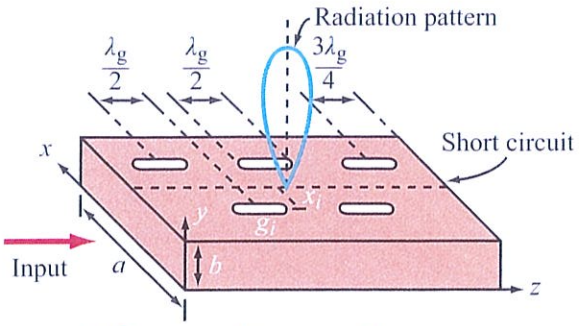

(a) Resonant slot array, with maximum radiation in broadside direction (y)

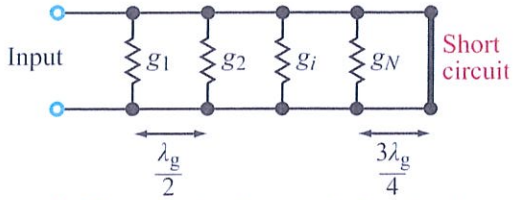

(b) Transmission-line equivalent circuit

Figure 3-37: The resonant slot array.

phase distributions among the array elements. An array consisting of longitudinal slots cut in the broad side of the waveguide (Fig. 3-37) has been found to exhibit negligible mutual coupling between adjacent slots (Ehrlich and Short, 1954). For the purpose of this introductory presentation, the discussion to follow is limited to this type of configuration, and the rectangular waveguide is assumed to be excited in the dominant TE_{10} mode.

Longitudinal slot arrays are commonly divided into two types: the ***resonant array*** and the ***nonresonant array***. A brief description of each follows.

Resonant array

The resonant array [Fig. 3-37(a)] is an in-phase array configured for broadside operation at a single frequency. For the slots to be excited in phase, they must be spaced one guide wavelength λ_g apart. In order to avoid grating lobes in the visible region of the array, the spacing between elements must be less than one free-space wavelength λ. Since in air-filled waveguides $\lambda_g > \lambda$, the λ_g spacing required for in-phase excitation results in grating lobes. The solution to this problem is to arrange the slots $\lambda_g/2$ apart with adjacent elements on opposite sides of the longitudinal axis of the waveguide, as shown in Fig. 3-37(a). The $\lambda_g/2$ spacing provides a phase difference of π between adjacent elements, and because the x component of the surface current flows in opposite directions on the two sides of the longitudinal axis, an additional phase difference of π is introduced in the excitation between adjacent slots. Thus, the slots are excited in phase, and if the guide dimensions are such that $\lambda_g/2 < \lambda$, grating lobes do not occur.

The transmission-line equivalent of the slot array is shown in Fig. 3-37(b). Associated with the ith slot is a ***shunt conductance*** g_i, whose magnitude is given by (Compton and Collin, 1969b)

$$g_i = K \sin^2\left(\frac{\pi x_i}{a}\right), \tag{3.111}$$

where K is a constant and x_i is the displacement of the slot from the longitudinal axis as shown in Fig. 3-37(a). The constant K is related to the waveguide dimensions a and b and to the wavelengths λ and λ_g. For a given voltage across the transmission line, the power radiated by a given slot is proportional to its conductance g_i, and hence to the displacement x_i. Thus, a desired amplitude distribution of the element feeding coefficients can be achieved by specifying the displacements x_i of the array slots. Since the amplitude distribution is usually defined in terms of the excitation field (or current) rather than power, the slot displacements should be chosen so that the desired relative amplitudes are proportional to $\sqrt{g_i}$, or $\sin(\pi x_i/a)$. Finally, by terminating the waveguide in a short circuit at a distance of $3\lambda_g/4$ from the last slot, such a termination translates to an open circuit at the last slot, thereby having no effect on its conductance. To satisfy this condition and to maintain the excitations of the slots in phase with one another, the array design is configured for operation at a single frequency, which has led to the name "resonant array." Consequently, a resonant slot array has a small bandwidth, typically on the order of $\pm 50\%/N$, where N is the number of slots.

Nonresonant array

Unlike the fixed-frequency broadside resonant array, the nonresonant array usually is designed for operation over a large bandwidth so that the direction of the mainlobe of the antenna array can be steered electronically by changing the frequency of the input signal. The array shown in Fig. 3-38 is terminated in a matched load to avoid reflections. Since part of the input power now is absorbed in the matched load, the nonresonant array is less efficient than the resonant array, but on the other hand, the use of the matched load allows operation over a much wider frequency range than is possible with the resonant array.

A constant spacing d between adjacent slots results in progressive (linear) phase shift along the array. If the wavelength of the input signal is such that d corresponds to $\lambda_g/2$, then the elements are excited in phase and the resultant beam is in the broadside direction ($\theta_0 = \pi/2$ in Fig. 3-38). In the general case, however, the beam angle θ_0 is governed by the relationship

$$\cos\theta_0 = \frac{\lambda}{\lambda_g} - \frac{\lambda}{2d}, \tag{3.112}$$

and for the TE_{10} mode in an unloaded waveguide

$$\frac{\lambda}{\lambda_g} = \sqrt{1 - \left(\frac{\lambda}{2a}\right)^2}. \tag{3.113}$$

Thus, the nonresonant slot array is amenable to frequency scanning wherein the mainlobe of the array is made to scan in the y–z plane by changing the frequency of the input signal. For more details regarding the design of slot arrays, the reader is referred to Compton and Collin (1969b), Balanis (2008), and Croswell (2007).

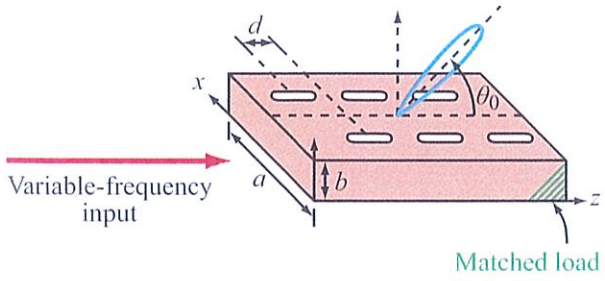

Figure 3-38: With the nonresonant slot array, the main beam may be steered in direction by varying the frequency of the input signal.

3-12.3 Microstrip Antennas

A microstrip antenna consists of a flat metallic patch separated from a ground conducting plane by a thin, uniform, nearly lossless dielectric substrate. Figure 3-39 shows a cross-sectional view of a microstrip antenna fed by a coaxial transmission line, with the center conductor of the coaxial line connected to the patch and the outer conductor connected to the ground plane. Alternatively, the microstrip antenna can be fed by other types of transmission lines, such as the microstrip line shown in Fig. 3-40. Because it can be inexpensively fabricated using printed circuit technology, both singly and in arrays, the microstrip antenna dominates the mobile phone market and is used extensively in many microwave applications. Disadvantages include low power-handling capability and a narrow bandwidth ($\approx$ 1–5%).

The patch of the microstrip antenna is typically rectangular or circular in shape, although other shapes are also used. For a rectangular patch, its length L is usually in the range $\lambda_0/3 < L < \lambda_0/2$, where λ_0 is the free-space wavelength. Its width W may vary over a wider range, typically $0.25\lambda_0 \leq W \leq 0.75\lambda_0$. The height h of the dielectric substrate, which influences both the bandwidth and radiation efficiency of the antenna, is usually in the range $0.003\lambda_0 \leq h \leq 0.05\lambda_0$. The rationale for these ranges will become evident in the next few paragraphs.

The radiation pattern of the microstrip patch antenna consists primarily of a broad single lobe, similar to that of a half-wave dipole. A typical example is shown in Fig. 3-41. If configured into a one-dimensional array, as depicted by Fig. 3-42, the overall pattern becomes much narrower in the plane containing the array axis and the normal to the antenna surface, and if arrayed into a two-dimensional lattice, the beam can be narrowed into a conical beam. To avoid grating lobes, the spacing between adjacent patches should be less than $\lambda_0/2$. Also, in the ***corporate feed network*** shown in

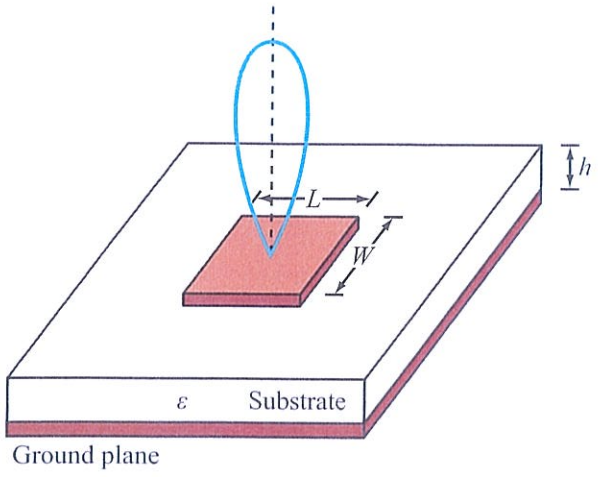

(a) Microstrip antenna

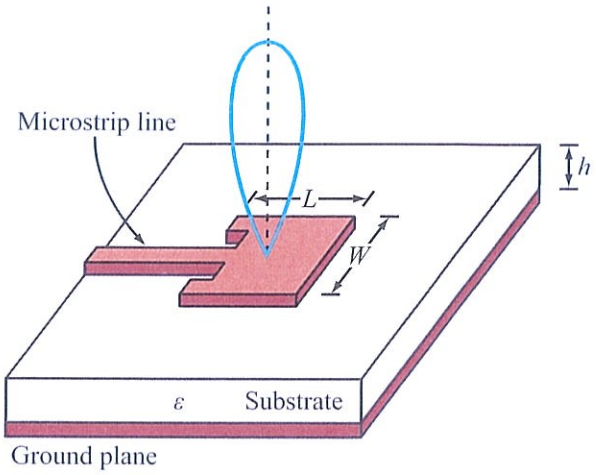

Figure 3-40: Microstrip patch antenna fed by a microstrip transmission line.

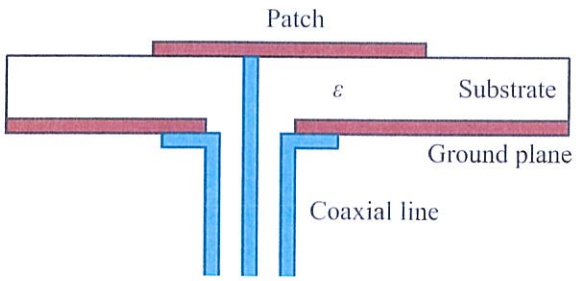

(b) Side view with coaxial feed line

Figure 3-39: (a) Top view of a rectangular patch antenna and (b) side view showing how it connects to a coaxial transmission line.

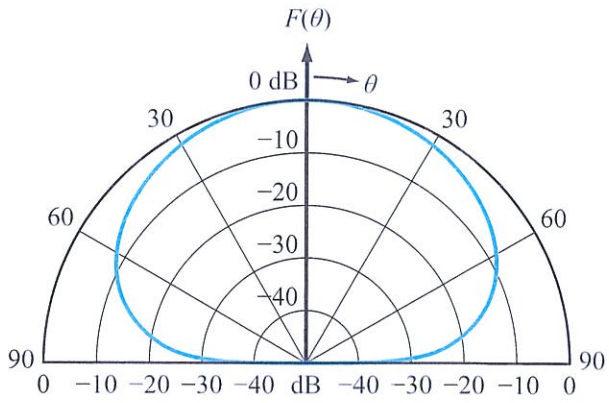

Figure 3-41: Far-field patterns of a rectangular patch on an infinite ground plane (Jackson, 2007).

Fig. 3-42, quarter-wave transformers are used to match the impedances of the individual antenna elements to a common 50-Ω microstrip transmission line.

Using electromagnetic simulation models (Jackson and Oliner, 2007; Balanis, 2008) it is possible to select the antenna and substrate dimensions so that the antenna input impedance $\mathbf{Z}_i$ provides a good match to the transmission line feed at a specific frequency of interest. In the example shown in Fig. 3-43, $\mathbf{Z}_i = (50 + j0)\ \Omega$ at $f = 1.575$ GHz, which is an ideal match to a 50-Ω transmission line, but $\mathbf{Z}_i$ varies rapidly with frequency. A small deviation away from 1.575 GHz causes both the real and imaginary components of $\mathbf{Z}_i$ to change significantly. The operational fractional bandwidth is defined as

$$\text{BW} = \frac{f_2 - f_1}{f_r}, \tag{3.114}$$

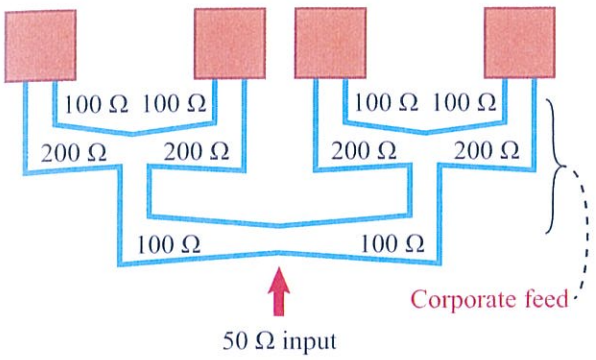

Figure 3-42: Tapered lines to match 100-Ω patches to a 50-Ω line (R. E. Munson, 1974).

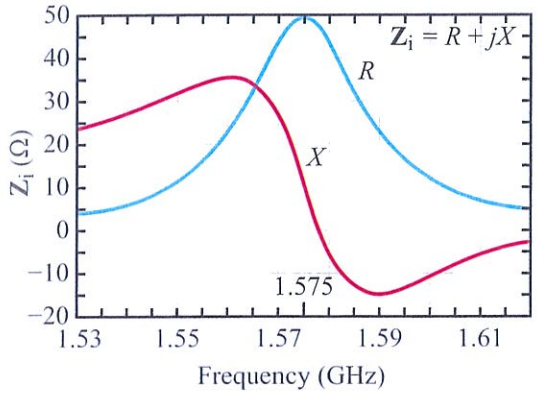

Figure 3-43: Input impedance $\mathbf{Z}_i$ of a microstrip antenna with $L = 6.255$ cm, $W = 9.383$ cm, $h = 0.1524$ cm, and $\varepsilon_r = 2.2$ (Jackson, 2007).

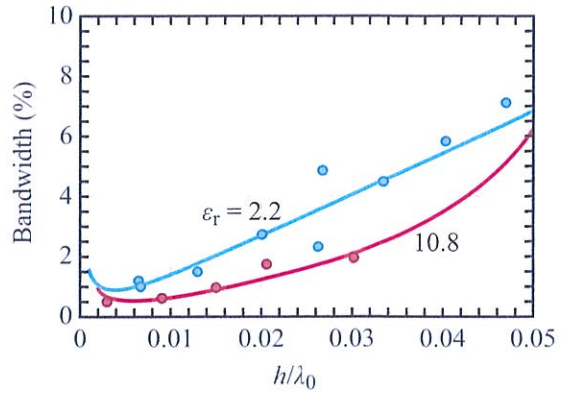

(a) Bandwidth

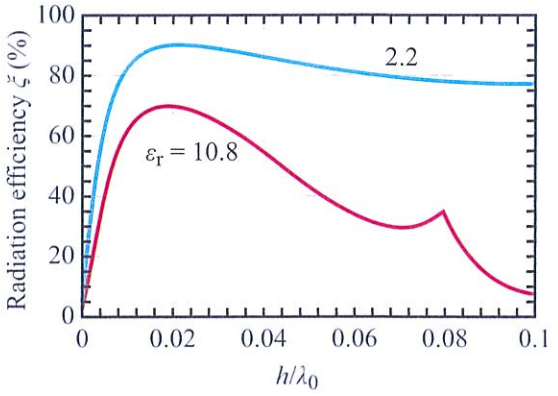

(b) Radiation efficiency

Figure 3-44: (a) Bandwidth and radiation efficiency versus the normalized substrate thickness for a moderate-permittivity substrate and a high-permittivity substrate (Jackson, 2007).

where f_r is the resonant frequency (1.575 GHz, in the present case), and f_1 and f_2 are the frequencies below and above f_r at which the impedance mismatch between the antenna and the transmission line is characterized by a standing wave ratio of a specified value, typically $S = 2$. Figure 3-44(a) displays the variation of percent fractional bandwidth as a function of h/λ_0, where h is the height of the dielectric substrate. The bandwidth increases with h/λ_0. However, beyond $h/\lambda_0 = 0.015$, the radiation efficiency ξ exhibits a decreasing trend with h/λ_0 [Fig. 3-44(b)]. Ultimately, the antenna dimensions and the height and permittivity of its substrate are selected by the antenna designer through a trade-off analysis to suit the intended application.

3-13 Active Antennas

As previously noted, while most antennas obey reciprocity, a particularly important class of antennas may not: those that contain active elements. Antennas containing active electronic components are known as

active antennas. In this context, an active antenna should not be confused with the "active" elements in a Yagi-Uda dipole array antenna (Yagi, 1928). In a Yagi-Uda array, some of the elements are not connected to the antenna feed but are parasitic elements designed to improve the antenna directivity. The passive elements are termed "directors" or "relectors" depending on their place in the array. In such antennas, the antenna elements connected to the antenna feed are commonly referred to as the active elements (Pozar, 1997). Old-style television antennas are good examples of Yagi-Uda antennas. In this book we define an active antenna as one that contains active electronic elements.

An active antenna is generally an array antenna in which transmit and receive amplifiers are distributed throughout the array. Figure 3-45 illustrates the difference between a conventional phased array antenna and an active array antenna. In a conventional phased array, the array elements are connected to phase shifters fed through a corporate (divided) feed and a ***transmit/receive*** (T/R) switch that selects between a ***high-power transmit amplifier*** (HPA) and a ***low-noise receive amplifier*** (LNA), which are connected to the upconverter and downconverter, respectively. (Up- and downconverters are discussed in Chapters 13 and 14.)

In the active antenna diagrammed in Fig. 3-45(b), each array element is fed from a dedicated transmit/receive module (TRM). These are connected by a corporate feed to a transmit/receive switch connected to the upconverter and the downconverter. The same upconverter and downconverter designs can be used in both the phased-array and the active antenna array. A diagram of a typical TRM is shown in Fig. 3-46, though some TRMs do not contain all components. For example, a receive-only active antenna would obviously not contain transmit amplifiers. Each TRM includes its own LNA and a power amplifier (PA), as well as T/R switches or circulators. In some applications a calibration feedback circuit is included to enable feeding some of the transmitted signal into the LNA (see Chapter 13). TRMs may contain phase shifters and variable-gain amplifiers to permit dynamic beam steering and beam shaping. The TRM includes power conditioning for the electronics and control logic for

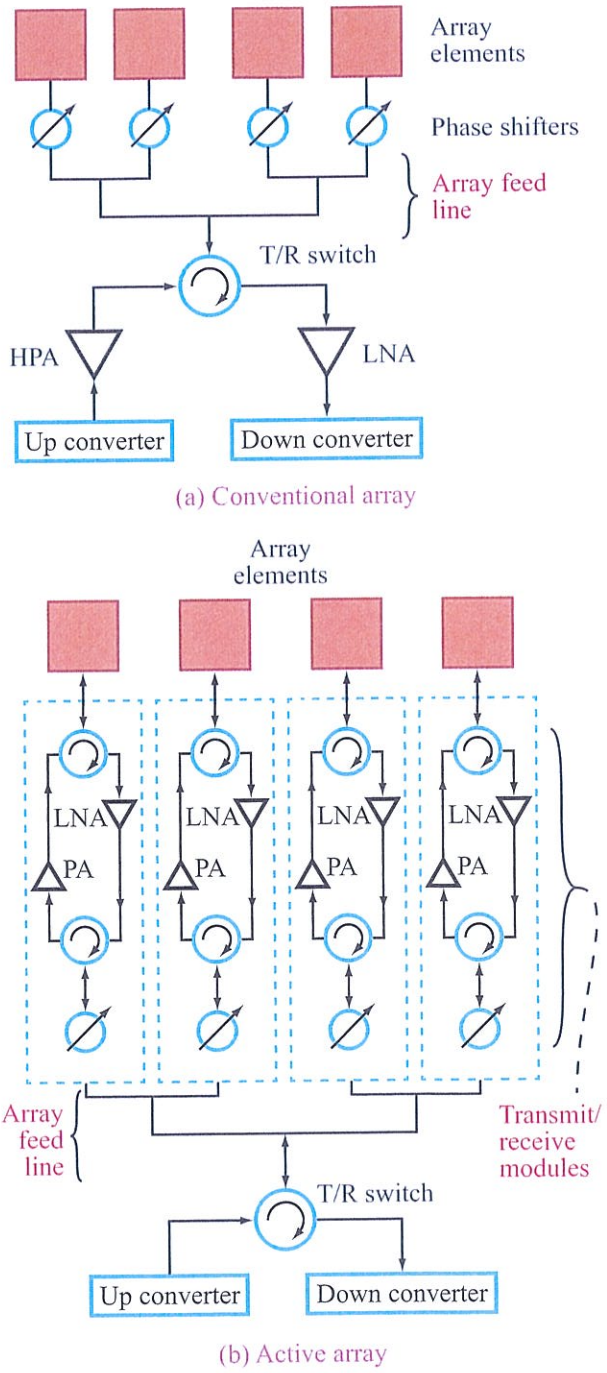

Figure 3-45: Comparison of (a) conventional and (b) active array system.

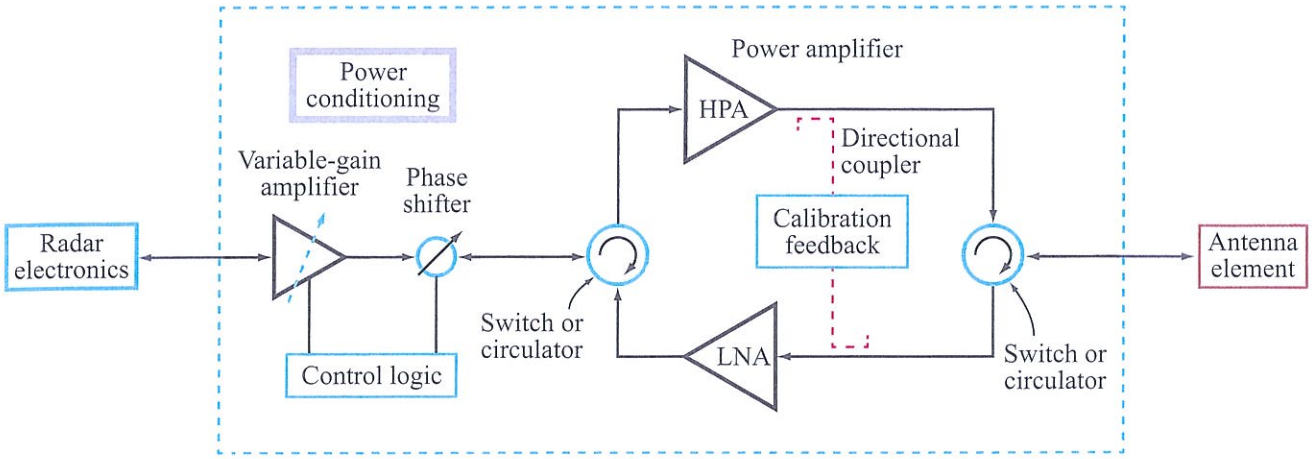

Figure 3-46: Design of an active transmit/receive module.

setting the gain of the variable-gain amplifier and phase of the phase shifter and for controlling the T/R switches and the calibration circuit.

3-13.1 Advantages of Active Antennas

Given the significant complexity that active antennas have in comparison with conventional passive antennas, why would one want to use an active antenna? In the following we explore some of the trade-offs between active and passive antennas.

Note that for a conventional antenna, the radiated power must be generated by one large HPA, and the feed structure and the phase shifters must be designed to handle high power levels. Also, the heat generated by the HPA is localized. In contrast, in an active antenna array, signal amplification is spread over multiple smaller amplifiers and the feeding and phase shifting occurs at much-smaller signal levels. These can reduce component cost and size, enable more rapid phase switching, and produce increased component reliability. The shorter signal paths between the antenna elements and the amplifiers result in less signal loss and thus in improved signal-to-noise ratio (SNR). Mass production of identical TRMs lower their cost. The savings can be used to reduce their size, weight, and power efficiency.

We also note that heat dissipation from the distributed amplifiers may be simplified and require less weight, a particular concern for spaceborne radar systems. The trade-off is the requirement that the TRMs must either have matched phase and gain or contain calibration and adjustment circuitry to ensure the achievement of the desired antenna performance. Due to thermal variations in amplifier gain and phase shifter performance, self-calibration and correction is essential in spaceborne systems.

Active antenna systems generally have higher fault tolerance: the failure of an amplifier has less effect in an active antenna. There is a trade-off, however, because there are many more individual electronic components in an active antenna system that can fail than in a system with a conventional passive antenna with fewer electronic elements. Due to the potentially higher mass of an active antenna compared with a passive one, the supporting structure requirements for the antenna system may be higher for an active antenna than for a passive antenna of the same performance. Finally, another disadvantage of an active antenna is that there is less room for high performance front-end filters (those between the antenna and LNA) in the TRM to minimize interference from undesired signals, so the front-end

filter performance may be reduced, which can result in increased sensitivity to interference.

Though higher in cost and complexity, the improved performance of active antennas have led to their use in spaceborne SAR systems such as ASAR on Envisat (Desnos et al., 2000), RADARSAT-2 (Riendeau and Grenier, 2007), and TerraSAR-X (Buckreuss et al., 2008). As technology continues to improve the performance of TRMs, while shrinking their size and cost, it is expected that active antennas will become increasingly more common.

3-13.2 Digital Beamforming with Active Antennas

The active phased-array antenna considered thus far forms only a single antenna beam based on analog summation of the phase-shifted receive signals in the feed, as illustrated in Fig. 3-47(a). After summation, the signal is amplified, filtered, downconverted, and digitized with an analog-to-digital (A/D) converter for digital processing. This requires only a single LNA, downconverter, and A/D converter. An alternative architecture, known as ***digital beamforming***, is illustrated in Fig. 3-47(b).

In a digital beamformer each antenna array element has a dedicated receiver that includes an LNA, filtering, downconversion, and an A/D. The digital data stream from each A/D is then summed in a digital summer processor. Any required phase shift or time delay is included in the digital summer output to produce precisely the same signal as in the analog beamformer. However, using a digital processor, multiple summations, each with a different phase distribution. This produces multiple simultaneous beams which can be steered independently. These can be used to provide wider coverage at the expense of increased complexity, cost, and data rate. Digital processing provides finer and faster control of beam steering and beam shaping than conventional analog beamforming. Digital beamforming offers the same SNR advantage as other active antennas with short antenna element-to-LNA paths. Elimination of the analog phase shifters and feed structure reduces antenna mass and simplifies calibration of the array. Finally, a digital beamformer has improved dynamic range since

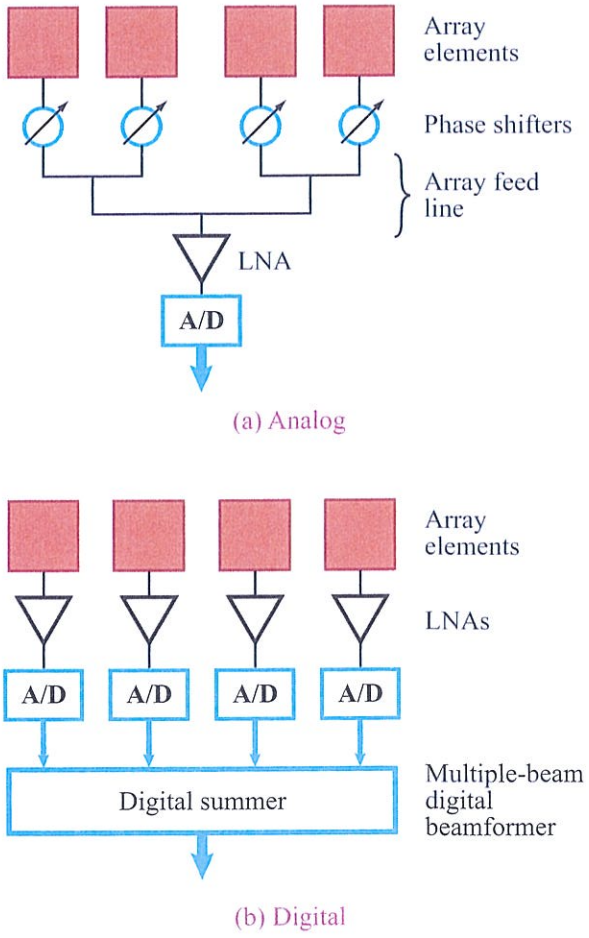

Figure 3-47: Comparison of (a) analog and (b) digital beamforming.

the signal level at the LNA is smaller. The coherent signal increase due to coherent summation over the aperture now occurs in the digital processor. The resulting increase in dynamic range can be handled digitally.

Note that digital beamforming can also be used for the transmit function by replacing A/Ds with digital-to-analog converters (D/As), the downconverter with an upconverter, and LNAs with HPAs. A single transmit beam can be formed and it can be steered rapidly. Using multiple orthogonal signals makes it possible to generate multiple simultaneous transmit beams, but specialized

digital processing of the received signal is required (Li and Stoica, 2009).

PROBLEMS

3.1 Determine the following:

(a) The direction of maximum radiation.

(b) Directivity.

(c) Beam solid angle.

(d) Half-power beamwidth in the x–z plane.

for an antenna whose normalized radiation intensity is given by

$$F(\theta,\phi) = \begin{cases} 1 & \text{for } 0 \le \theta \le 60^\circ \text{and } 0 \le \phi \le 2\pi \\ 0 & \text{elsewhere.} \end{cases}$$

Suggestion: Sketch the pattern prior to calculating the desired quantities.

3.2 Repeat Problem 3.1 for an antenna with

$$F(\theta,\phi) = \begin{cases} \sin^2\theta\cos^2\phi & \text{for } 0 \le \theta \le \pi \\ & \text{and } -\pi/2 \le \phi \le \pi/2 \\ 0 & \text{elsewhere} \end{cases}$$

3.3 An antenna with a pattern solid angle of 1.5 (sr) radiates 60 W of power. At a range of 1 km, what is the maximum power density radiated by the antenna?

3.4 An antenna with a radiation efficiency of 90% has a directivity of 7.0 dB. What is its gain in decibels?

3.5 The radiation pattern of a circular parabolic-reflector antenna consists of a circular major lobe with a half-power beamwidth of 3° and a few minor lobes. Ignoring the minor lobes, obtain an estimate for the antenna directivity in dB.

3.6 The normalized radiation intensity of a certain antenna is given by

$$F(\theta) = \exp(-20\theta^2) \qquad \text{for } 0 \le \theta \le \pi,$$

where θ is in radians. Determine:

(a) The half-power beamwidth.

(b) The pattern solid angle.

(c) The antenna directivity.

3.7 A 3 GHz line-of-sight microwave communication link consists of two lossless parabolic dish antennas, each 1 m in diameter. If the receive antenna requires 10 nW of receive power for good reception and the distance between the antennas is 40 km, how much power should be transmitted?

3.8 Consider the communication system shown in Fig. P3.8, with all components properly matched. If $P_t = 10$ W and $f = 6$ GHz:

(a) What is the power density at the receiving antenna (assuming proper alignment of antennas)?

(b) What is the received power?

(c) If the receiver noise power is $P_n = KT_{sys}B$, where K is Boltzmann's constant (1.38×10^{-23} J/K), $T_{sys} = 1000$ K is the receiver system temperature, and the receiver bandwidth is $B = 20$ MHz, what is the signal-to-noise ratio in decibels?

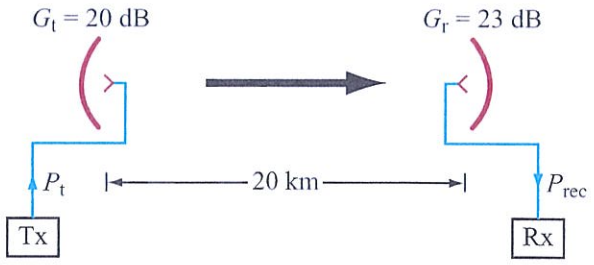

Figure P3.8: Communication system of Problem 3.8.

3.9 A uniformly illuminated aperture is of length $l_x = 20\lambda$. Determine the beamwidth between first nulls in the x–z plane.

3.10 The 10 dB beamwidth is the beam size between the angles at which $F(\theta)$ is 10 dB below its peak value. Determine the 10 dB beamwidth in the x–z plane for a uniformly illuminated aperture with length $l_x = 10\lambda$.

3.11 A uniformly illuminated rectangular aperture situated in the x–y plane is 2 m high (along x) and 1 m wide (along y). If $f = 10$ GHz, determine the following:

(a) The beamwidths of the radiation pattern in the elevation plane (x–z plane) and the azimuth plane (y–z plane).

(b) The antenna directivity D in decibels.

3.12 An antenna with a circular aperture has a circular beam with a beamwidth of 3° at 20 GHz.

(a) What is the antenna directivity in dB?

(b) If the antenna area is doubled, what will be the new directivity and new beamwidth?

(c) If the aperture is kept the same as in (a), but the frequency is doubled to 40 GHz, what will the directivity and beamwidth become then?

3.13 A 94 GHz automobile collision-avoidance radar uses a rectangular-aperture antenna placed above the car's bumper. If the antenna is 15 cm in length and 5 cm in height, determine the following:

(a) Its elevation and azimuth beamwidths.

(b) The horizontal extent of the beam at a distance of 300 m.

3.14 A microwave telescope consisting of a very sensitive receiver connected to a 100 m parabolic-dish antenna is used to measure the energy radiated by astronomical objects at 20 GHz. If the antenna beam is directed toward the moon and the moon extends over a planar angle of 0.5° from Earth, what fraction of the moon's cross section will be occupied by the beam?

3.15 Derive an expression for the far-zone normalized radiation pattern of a rectangular aperture with dimensions a and b, illuminated by

(a)

$$E_a(x_a, y_a) = \begin{cases} E_0 \cos\left(\dfrac{\pi x_a}{a}\right) & \text{for } |x_a| \le \dfrac{a}{2} \text{ and } |y_a| \le \dfrac{b}{2}, \\ 0 & \text{otherwise,} \end{cases}$$

(b)

$$E_a(x_a, y_a) = \begin{cases} \dfrac{E_0}{2}\left[1 + \cos\left(\dfrac{\pi x_a}{a}\right)\right] & \text{for } |x_a| \le \dfrac{a}{2} \text{ and } |y_a| \le \dfrac{b}{2}, \\ 0 & \text{otherwise.} \end{cases}$$

(c) Plot the x–z-plane radiation patterns of the uniformly illuminated aperture and the above two apertures. Compare half-power beamwidths and sidelobe levels.

3.16 Find the far-field radiation pattern of a Gaussianly illuminated rectangular aperture, with

$$E_a(x_a, y_a) = \begin{cases} \dfrac{1}{\sqrt{2\pi\sigma^2}} \exp\left(\dfrac{-\pi x_1^2}{2\sigma^2}\right) & \text{for } |x_1| \le 1 \text{ and } |y_1| \le 1, \\ 0 & \text{otherwise,} \end{cases}$$

where $x_1 = 2x_a/a$ and $y_1 = 2y_a/b$.

3.17 A rectangular aperture is illuminated by the function

$$E_a(x_a, y_a) = \begin{cases} E_0 f(x_1) & \text{for } |x_1| \le 1 \text{ and } |y_1| \le 1, \\ 0 & \text{otherwise,} \end{cases}$$

where $f(x_1)$ is shown below, and x_1 and y_1 are as defined in Problem 3.16.

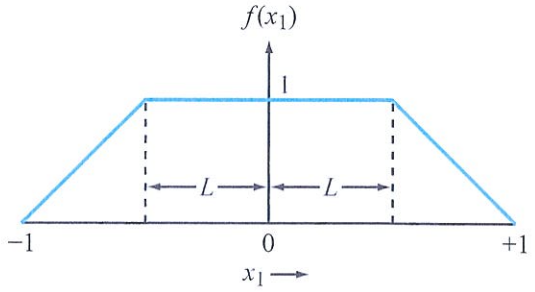

Figure P3.17: Figure for Problem 3.17.

(a) Express $f(x_1)$ as a convolution of two rectangular functions: $f(x_1) = f_1(x_1) * f_2(x_1)$.

(b) Use the convolution property of the Fourier transform to obtain the normalized radiation pattern of the aperture.

3.18 A two-element array consisting of two isotropic antennas separated by a distance d along the z axis is placed in a coordinate system whose z axis points

eastward and whose x axis points toward the zenith. If a_0 and a_1 are the amplitudes of the excitations of the antennas at $z = 0$ and at $z = d$, respectively, and if δ is the phase of the excitation of the antenna at $z = d$ relative to that of the other antenna, find the array factor and plot the pattern in the x–z plane for the following:

(a) $a_0 = a_1 = 1$, $\delta = \pi/4$, and $d = \lambda/2$

(b) $a_0 = 1$, $a_1 = 2$, $\delta = 0$, and $d = \lambda$

(c) $a_0 = a_1 = 1$, $\delta = -\pi/2$, and $d = \lambda/2$

(d) $a_0 = 1$, $a_1 = 2$, $\delta = \pi/4$, and $d = \lambda/2$

(e) $a_0 = 1$, $a_1 = 2$, $\delta = \pi/2$, and $d = \lambda/4$

3.19 Find and plot the normalized array factor and determine the half-power beamwidth for a five-element linear array excited with equal phase and a uniform amplitude distribution. The interelement spacing is $3\lambda/4$.

3.20 A five-element, equally spaced linear array with $d = \lambda/2$ is excited with uniform phase and an amplitude distribution given by the binomial distribution

$$a_i = \frac{(N-1)!}{i!(N-i-1)!}, \qquad i = 0, 1, \ldots, (N-1),$$

where N is the number of elements. Develop an expression for the array factor.

3.21 A three-element linear array of isotropic sources aligned along the z axis has an interelement spacing of $\lambda/4$ (Fig. P3.21). The amplitude excitation of the center element is twice that of the bottom and top elements, and the phases are $-\pi/2$ for the bottom element and $\pi/2$ for the top element, relative to that of the center element. Determine the array factor and plot it in the elevation plane.

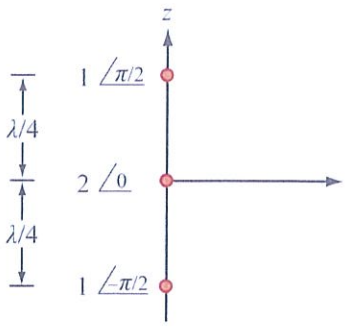

Figure P3.21: Three-element array of Problem 3.21.

3.22 An eight-element linear array with $\lambda/2$ spacing is excited with equal amplitudes. To steer the main beam to a direction 60° below the broadside direction, what should be the incremental phase delay between adjacent elements? Also, give the expression for the array factor and plot the pattern.

3.23 A linear array arranged along the z axis consists of 12 equally spaced elements with $d = \lambda/2$. Choose an appropriate incremental phase delay δ so as to steer the main beam to a direction 30° above the broadside direction. Provide an expression for the array factor of the steered antenna and plot the pattern. From the pattern, estimate the beamwidth.

3.24 Design a 3 cm wavelength optimum pyramidal horn, given the constraint that the axial length l_0 cannot exceed 30 cm. Find its maximum directivity D_p.

3.25 A square aperture with dimensions much larger than λ is illuminated by a cosine amplitude distribution with $n = 1$ along both dimensions, thereby generating an approximately azimuthally symmetric radiation pattern. Use the x–z pattern to calculate the beam efficiency of the antenna.

3.26 A square aperture with dimensions much larger than λ is illuminated by a cosine amplitude distribution with $n = 2$ along both dimensions, thereby generating an approximately azimuthally symmetric radiation pattern. Use the x–z pattern to calculate the beam efficiency of the antenna.

3.27 A square aperture with dimensions much larger than λ is illuminated by a triangular amplitude

distribution along both dimensions, thereby generating an approximately azimuthally symmetric radiation pattern. Use the x–z pattern to calculate the beam efficiency of the antenna.

3.28 Designers of a 5.4 GHz SAR are choosing between an active antenna and a conventional array. To achieve the desired beam pattern, the aperture size is 15 m $\times$ 1.4 m. For a two-dimensional array of microstrip patches with $\lambda/2$ element spacing and assuming one TRM per patch with a TRM transmit power of 1 W/element, what is the minimum HPA output power required from a conventional array to achieve the same peak radiated power supplied by the active array? If the TRM transmit efficiency is 50% and the HPA efficiency is 75% but the HPA feed loss is 3 dB, what is the peak power required for each case?

3.29 How is the antenna pattern affected by the failure of a single TRM in a 16-element linear array with spacing $d = \lambda/2$? For simplicity, assume that the failure occurs in one of the end elements and the beam is steered to broadside. Sketch the difference in the antenna pattern before and after the failure.

3.30 Assume a plane-wave signal incident upon an 8-element linear phased array ($d = \lambda/2$) at an angle of 30°. Compute the signal level of the output of the antenna feed when (a) the antenna is steered to broadside and (b) when it is steered at 30° toward the signal source. What does your analysis indicate about the dynamic range of a phased-array antenna?

Code 3.2 **Array Factor for Uniformly Spaced Array with Linear Phase Distribution**

This module computes the array factor as defined by Eq. (3.97) for an N-element uniformly spaced array whose elements are radiating with phases that are linearly related to each other. The user specifies the change in phase between the elements, in degrees, as well as each of the amplitudes. The physical spacing of the elements is specified by the user in wavelengths.

matlab code: ArrayFactor_LinearPhaseDist.m

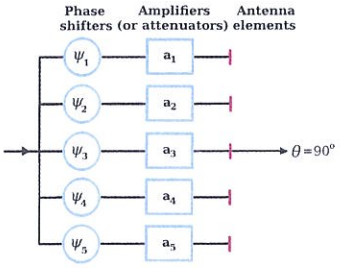

Element 1 Amplitude:	5
Element 2 Amplitude:	7
Element 3 Amplitude:	10
Element 4 Amplitude:	7
Element 5 Amplitude:	5
Incremental Phase Delay (deg):	0
Element Spacing, wavelengths:	0.5

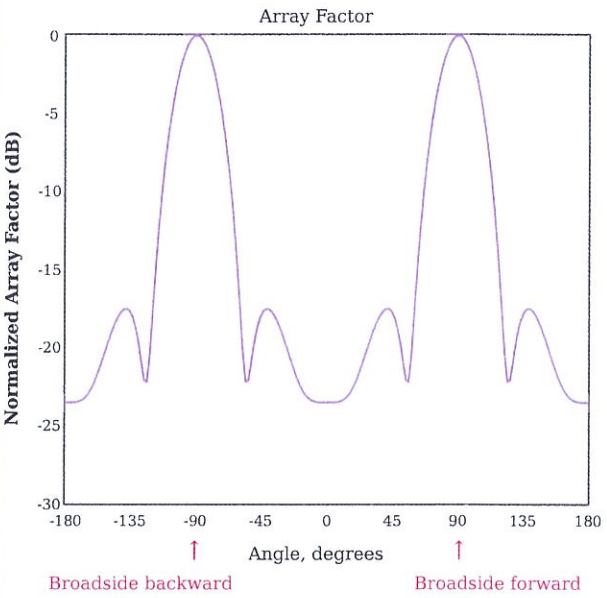

An example of one of the interactive modules available at the book website: mrs.eecs.umich.edu.